

**U.S. DEPARTMENT OF COMMERCE
National Oceanic and Atmospheric Administration
Environmental Research Laboratories**

NOAA Technical Memorandum ERL NSSL-58

**THE THERMAL STRUCTURE OF THE LOWEST
HALF KILOMETER IN CENTRAL OKLAHOMA:
DECEMBER 9, 1966 - MAY 31, 1967**

R. Craig Goff
Horace R. Hudson

Property of
NWC Library
University of Oklahoma

National Severe Storms Laboratory
Norman, Oklahoma
July 1972



FOREWORD

The work reported here has received substantial support from the National Aeronautics and Space Administration. Their financial support assisted in the purchase and installation of conduit and temperature and wind sensors on the tower. Their sustaining support in the past years has aided in continuing the boundary layer investigations.

The transmitting tower of WKY-TV in Oklahoma City was made available to the National Severe Storms Laboratory for the installation of meteorological equipment through the cooperation of the management and engineers of WKY Television Systems, Inc.

TABLE OF CONTENTS

| | Page |
|------------------------------------------------------------------------------------|------|
| FOREWORD | ii |
| LIST OF FIGURES | v |
| LIST OF TABLES | vii |
| ABSTRACT | viii |
| | |
| 1. INTRODUCTION | 1 |
| 2. TEMPERATURE SYSTEM | 1 |
| 3. GENERAL TEMPERATURE CHARACTERISTICS | 3 |
| 4. GENERAL LAPSE RATE CHARACTERISTICS | 8 |
| 4.1 Hourly Means and Frequency Distributions | 8 |
| 4.2 Characteristics of Time Adjusted Data | 13 |
| 4.3 Thermal Stratification Versus Wind Characteristics | 24 |
| 4.4 Persistence | 26 |
| 5. INVERSION CHARACTERISTICS FOR DIFFERENT VARIABLES | 29 |
| 5.1 Frequency of Inversions by Hour and Layer | 29 |
| 5.2 Frequency of Inversions by Air Mass and Layer | 31 |
| 5.2.1 Air Mass Criteria for Oklahoma | 31 |
| 5.2.2 Application of Air Mass Criteria to Inversion Conditions | 32 |
| 5.3 Frequency of Inversions by Cloud Cover and Layer | 33 |
| 5.3.1 Cloud Cover Characteristics for Oklahoma | 33 |
| 5.3.2 Application of Cloud Cover Criteria to Inversion Conditions | 34 |
| 6. CASE STUDIES | 35 |
| 6.1 A Sequence of Changing Air Masses Associated With an Extra-tropical Cyclone | 35 |
| 6.2 A Warm Frontal Passage | 38 |
| 6.3 A Dissipating Inversion After Sunrise | 40 |
| 7. SPECTRUM ANALYSIS | 43 |
| 8. SUMMARY AND CONCLUSIONS | 45 |
| 9. ACKNOWLEDGMENTS | 46 |
| 10. REFERENCES | 47 |
| APPENDIX | 50 |

LIST OF FIGURES

| Figure | | Page |
|--------|-----------------------------------------------------------------------------------------------------------------------------------------------------------------------------------------------------------------------------------------------------------|-----------|
| 1 | Mean daily surface (2m) temperature ($^{\circ}\text{C}$). | 3 |
| 2 | Mean hourly temperature ($^{\circ}\text{C}$) for the whole sample. | 4 |
| 3 | Mean hourly temperatures ($^{\circ}\text{C}$): (a) December 1966, (b) January 1967, (c) February 1967, (d) March 1967, (e) April 1967, (f) May 1967. | 5- 7 |
| 4 | Mean hourly lapse rates ($-\partial T/\partial Z$ in $^{\circ}\text{C } 100 \text{ m}^{-1}$) for the whole sample. | 8 |
| 5 | Relative frequency distribution of lapse rate ($^{\circ}\text{C } 100 \text{ m}^{-1}$). Inserts give greater resolution around the dry adiabat (arrows): (a) 23 m, (b) 67 m, (c) 133 m, (d) 221 m, (e) 310 m, (f) 400 m. | 10- 11 |
| 6 | Lapse rate ($^{\circ}\text{C } 100 \text{ m}^{-1}$) versus time before/after sunset: (a) Whole sample, (b) cP air masses, (c) Clear cP air masses, (d) Cloudy cP air masses, (e) All mT air masses (f) Clear mT air masses, (g) cT air masses. | 14- 17 |
| 7 | Relative frequency of $\% \geq \delta_d$ versus time before/after sunset. | 19 |
| 8 | Lapse rate ($^{\circ}\text{C } 100 \text{ m}^{-1}$) versus time before/after sunrise: (a) Whole sample, (b) cP air masses, (c) Clear cP air masses, (d) Cloudy cP air masses, (e) mT air masses, (f) Clear mT air masses, (g) cT air masses. | 21- 24 |
| 9 | A sequence of changing air masses (21-24 April 1967). Isotachs in m sec^{-1} , isotherms in $^{\circ}\text{C}$. | 37 |
| 10 | Selected temperature profiles during the 31 January - 1 February '67 warm frontal passage. | 39 |
| 11 | Schematic diagram of the 31 January - February '67 warm front. | 39 |
| 12 | Temperature time section during a dissipating morning inversion. 12 February 1967. Temperatures in $^{\circ}\text{C}$. | 41 |

LIST OF TABLES

| Table | | Page |
|-------|-----------------------------------------------------------------------------------------------------------------------------------------------------------------------------------------------|------|
| 1 | Arithmetic mean and standard deviation of temperatures by month. (a) Arithmetic mean temperatures by month, (b) Standard deviation of the temperature by month. | 2 |
| 2 | Frequency distribution of lapse rate ($^{\circ}\text{C}/100\text{ m}$) for six layers and four stability groups. | 12 |
| 3 | Mean depth of the well-mixed layer. | 20 |
| 4 | Probability of wind speed for given wind direction at 23 and 400 m for four stability groups. | 25 |
| 5 | Thermal stratification versus speed shear for three layers (probabilities). | 27 |
| 6 | Persistence of lapse rate for six layers and four stability groups. | 28 |
| 7 | Frequency of inversion by hour and layer. (a) $\delta \leq 0^{\circ}\text{C } 100\text{ m}^{-1}$, (b) $\delta \leq -4^{\circ}\text{C } 100\text{ m}^{-1}$. | 30 |
| 8 | Air mass subgroups. | 31 |
| 9 | Relative frequency (percent) of inversions by air mass and layer. | 33 |
| 10 | Frequency of inversions by cloud cover group and layer. (a) $\delta \leq 0^{\circ}\text{C } 100\text{ m}^{-1}$, (b) $\delta \leq -4^{\circ}\text{C } 100\text{ m}^{-1}$. | 34 |
| 11 | Relative frequency (percent) of inversions by cloud cover group and layer. (a) $\delta \leq 0^{\circ}\text{C } 100\text{ m}^{-1}$, (b) $\delta \leq -4^{\circ}\text{C } 100\text{ m}^{-1}$. | 35 |

| Figure | | Page |
|--------|------------------------------------------------------------------------------------------------------------------------------|------|
| 13 | Lapse rate ($^{\circ}\text{C } 100 \text{ m}^{-1}$) time section during a dissipating morning inversion. 12 February 1967. | 41 |
| 14 | Preconvective and convective stages of a late morning inversion (schematic). | 42 |
| 15 | Profile changes during convective overshoot (schematic). | 42 |
| 16 | Band-pass filter for spectra. | 44 |
| 17 | Temperature spectra in the planetary boundary layer. (a) 2 m, (b) 90 m, (c) 444 m. | 45 |
| A-1 | Temperature strip chart in the ambient mode. | 51 |
| A-2 | Temperature strip chart in the delta mode. | 51 |
| A-3 | Nominal linearity correction for a typical thermistor (range -25°C to 50°C). | 51 |

ABSTRACT

Nearly six months of temperature data from a 450 m tower in central Oklahoma are analyzed for mean characteristics in time and height. Temporal analyses of the data are performed by centering data at local noon and by centering the data at sunrise and sunset. During the sunset transition there is a tendency for increased instability at the top of the tower following an afternoon period of apparent stability. During the morning transition, strong nocturnal inversions persist to the late morning hours. The boundary layer and the free atmosphere are not coupled in many cases until around local noon.

Data are also analyzed for their characteristic thermal stratifications in different air masses and under different sky conditions. Inversions are assumed to be caused by three principal factors in the boundary layer: radiation, subsidence, and advection. Each of these three factors affects the boundary layer differently in different air masses and sky conditions. The cloud cover has a pronounced effect on the magnitude of inversions near the surface but has little apparent effect near the top of the tower.

Three case studies of interesting meteorological phenomena are presented: two are concerned with the vertical structure of the boundary layer during frontal passages or air mass changes. In the warm front case study, a low-level inversion is shown to impede the downward progression of warm advection. In the second case study, a rapid sequence of six air mass changes in three days is illustrated with a time-height section of the wind and temperature and a time section of moisture and sky conditions. A third case study discusses salient features of a dissipating nocturnal inversion after sunrise. Initially, the inversion is rapidly dissipated by surface heating below the base of the inversion. After a superadiabatic layer below the base grows to a sufficient depth, however, convective elements tend to physically lift the inversion, while the erosion at the base continues.

Finally, spectrum analyses of the temperature at three levels indicate significant differences among the planetary, synoptic and subsynoptic scales. The planetary scale induces more variance at all levels than does the synoptic scale. The diurnal and semidiurnal variance is much reduced at the top of the tower, and assuming vertical extrapolation is valid, small scale variance is negligible at the top of the boundary layer (1000 m).

THE THERMAL STRUCTURE
OF THE LOWEST HALF KILOMETER IN CENTRAL OKLAHOMA:
DECEMBER 9, 1966 - MAY 31, 1967

R. Craig Goff and Horace R. Hudson
National Severe Storms Laboratory¹

1. INTRODUCTION

The National Severe Storms Laboratory (NSSL) established a meteorological tower facility at the WKY-TV transmitter tower in 1966 primarily to study meso-scale boundary layer features associated with thunderstorms. This tower is located in rolling terrain about 6 n mi north of Oklahoma City, Oklahoma. A detailed description of the tower site has been given by Sanders and Weber (1970).

In a recent study, Crawford and Hudson (1970) examined the general properties of winds in the 444 m tower layer using a one-year sample (June 1966 - May 1967). Temperature data for a portion of the same period (December 1966 - May 1967) are examined in this paper. These two reports provide a base for other boundary layer studies using data from this facility.

2. TEMPERATURE SYSTEM

Temperature data were obtained from seven levels at the WKY-TV tower site (5 min mean values centered at the start of each hour extracted from strip charts). The surface temperature was obtained at 2 m on a 7 m tower located about 80 m from the base of the taller tower. This tower is 60 m north of the WKY-TV transmitter building, and because of prevailing winds, the exposure is not considered representative of the general surface wind characteristics. The temperature is affected to a much smaller degree. The other temperatures were recorded at six levels (45, 90, 177, 266, 355, and 444 m) on the main tower. Temperatures are measured with Yellow Springs Instruments linearized thermistor composites in aspirated shields. The average measured time constant of the thermistor probes in free air is about 30 sec (Carter, 1970).

Predetermined temperature corrections must be added to the raw data to obtain true temperatures. These corrections are a non-linear function of the true temperature. They are determined in the laboratory before and after data collection and are found not to change significantly for periods up to several months. Specific details concerning the application of the temperature corrections and quality control techniques used prior to data analysis are given in the Appendix.

¹ Mr. Hudson is presently employed at the National Severe Storms Forecast Center, Kansas City, Missouri.

Table 1. Arithmetic Mean and Standard Deviation of Temperatures by Month

| (a) Arithmetic Mean Temperatures by Month | | | | | | | |
|-------------------------------------------|----------------|------|------|-------|-------|-------|----------|
| Height (m) | Dec. (23 days) | Jan. | Feb. | Mar. | Apr. | May | Data Set |
| 444 | 2.83 | 5.35 | 3.66 | 12.21 | 15.82 | 16.87 | 9.80 |
| 355 | 2.90 | 5.37 | 3.91 | 12.43 | 16.21 | 17.34 | 10.06 |
| 266 | 2.92 | 5.31 | 4.21 | 12.72 | 16.60 | 17.76 | 10.29 |
| 177 | 2.95 | 5.25 | 4.22 | 12.95 | 17.07 | 18.15 | 10.50 |
| 90 | 2.83 | 5.16 | 4.76 | 13.08 | 17.53 | 18.47 | 10.69 |
| 45 | 2.55 | 5.08 | 4.89 | 13.18 | 17.81 | 18.56 | 10.74 |
| 2 | 1.71 | 4.49 | 4.62 | 12.99 | 17.96 | 18.34 | 10.43 |
| Mean temps* | 4.4 | 2.8 | 4.8 | 9.2 | 15.5 | 20.2 | 9.8 |
| Departure** | -2.7 | +1.7 | -0.2 | + 3.8 | + 2.5 | - 1.9 | + .6 |

(b) Standard Deviation of the Temperature by Month

| | | | | | | | |
|-----|------|------|------|------|------|------|------|
| 444 | 7.84 | 7.63 | 6.89 | 8.64 | 4.95 | 5.58 | 9.02 |
| 355 | 8.03 | 7.44 | 6.90 | 8.73 | 4.89 | 5.61 | 9.11 |
| 266 | 8.06 | 7.33 | 6.80 | 8.75 | 4.84 | 5.57 | 9.17 |
| 177 | 7.92 | 7.32 | 6.50 | 8.69 | 4.84 | 5.54 | 9.23 |
| 90 | 7.68 | 7.40 | 6.59 | 8.55 | 4.89 | 5.53 | 9.28 |
| 45 | 7.44 | 7.47 | 6.58 | 8.54 | 4.97 | 5.58 | 9.36 |
| 2 | 7.23 | 7.78 | 6.79 | 8.68 | 5.17 | 5.93 | 9.65 |

* OKC climatological mean temperature

** Departure of 2 m mean temperatures from the OKC climatological data

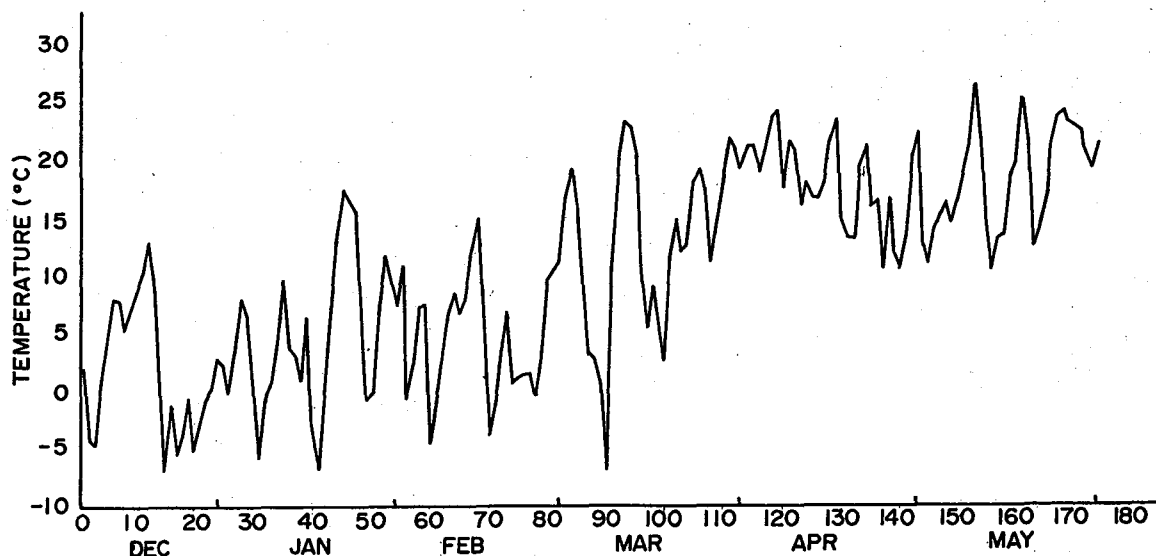


Figure 1. Mean daily surface (2m) temperature (°C).

3. GENERAL TEMPERATURE CHARACTERISTICS

Arithmetic mean temperatures and standard deviations were calculated by month and for the 6 month data set (Table 1a and b). The Oklahoma City 30-year mean monthly temperatures and the tower deviations from the Oklahoma City mean temperatures are given at the bottom of Table 1a. An observation was not included in the computation of the mean temperature if data from any level were missing. A rapid change from winter to spring is indicated by the difference in monthly averages between February and March². The quick transition is evident in figure 1, a plot of the mean temperatures by day (midnight to midnight). March has a large standard deviation as further evidence. As a result, the mean temperature of the entire sample is between those of the winter and spring regimes and is considerably different from those for any particular month.

It is interesting to note that the winter months exhibit considerable temperature variance, which is a maximum in mid-March just prior to the onset of the

² The monthly means at the tower (SFC level) are all within 1.2°C of the 1966-1967 means based on observations at the Oklahoma City (OKC) Weather Bureau Airport Station (U.S. Department of Commerce, 1966-7). This station is 11 n mi south-southwest of the tower. Climatological means (U.S. Department of Commerce, 1966-7) indicate that 3 months were above normal and 3 were below normal. The mean for the entire data set is 0.6°C above the climatological mean for this 174 day period.

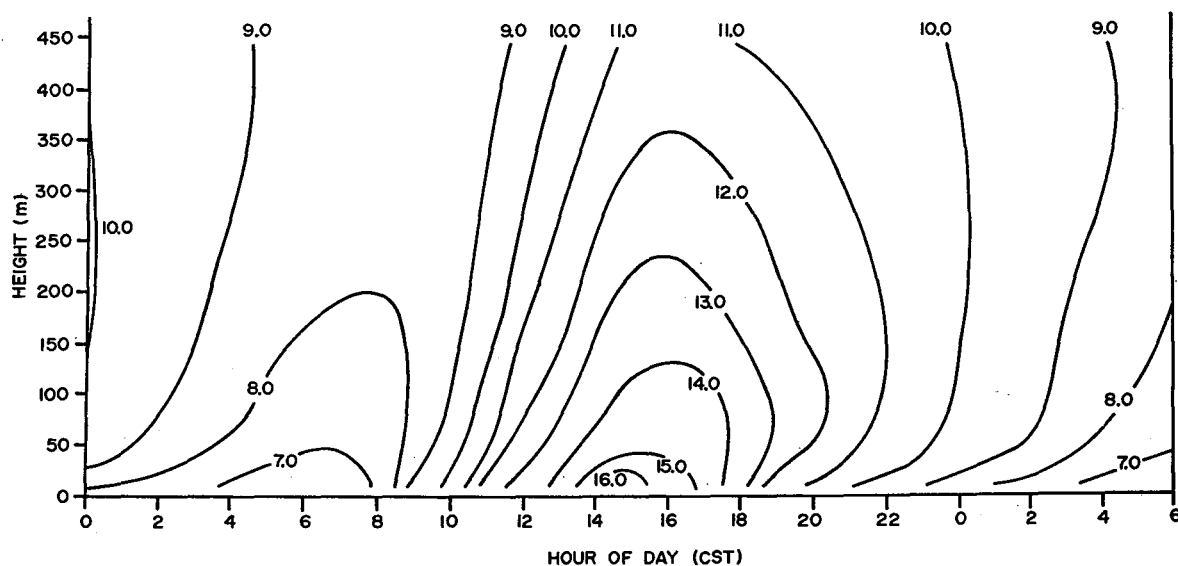


Figure 2. Mean hourly temperature ($^{\circ}\text{C}$) for the whole sample.

"spring regime." Thereafter, the variance is much reduced. It is believed that this is a rather typical type of transition from the winter to spring season in the Southern Great Plains.

Mean temperatures calculated by hour (fig. 2) show a mean surface temperature range from 6.2°C at 0600^3 to 16.6°C at 1500. At 444 m, mean temperatures range from 8.4°C at 1000 to 11.3°C at 1600, a significant reduction in the diurnal variation compared with the low-level variation and a shift in phase of the temperature wave. The phase shift in the temperature wave is in agreement with Sutton (1953) and others.

Several hours of insolation are needed before the effects of heating are observed at higher levels. Diurnal heating which begins first at the surface does not affect levels above 300 m until several hours later.

A thin layer nearest the ground is heated very quickly after sunrise, reversing the pre-sunrise inversion. This is accomplished by molecular heat transfer (conduction). Conductive processes, however, have a very small vertical scale and give way to convective process a short distance above the surface. Convection is responsible for transporting heat higher into the planetary boundary layer. The greater the height of the layer heated, the slower the heating process, since the

³ All times in this report are Central Standard Time.

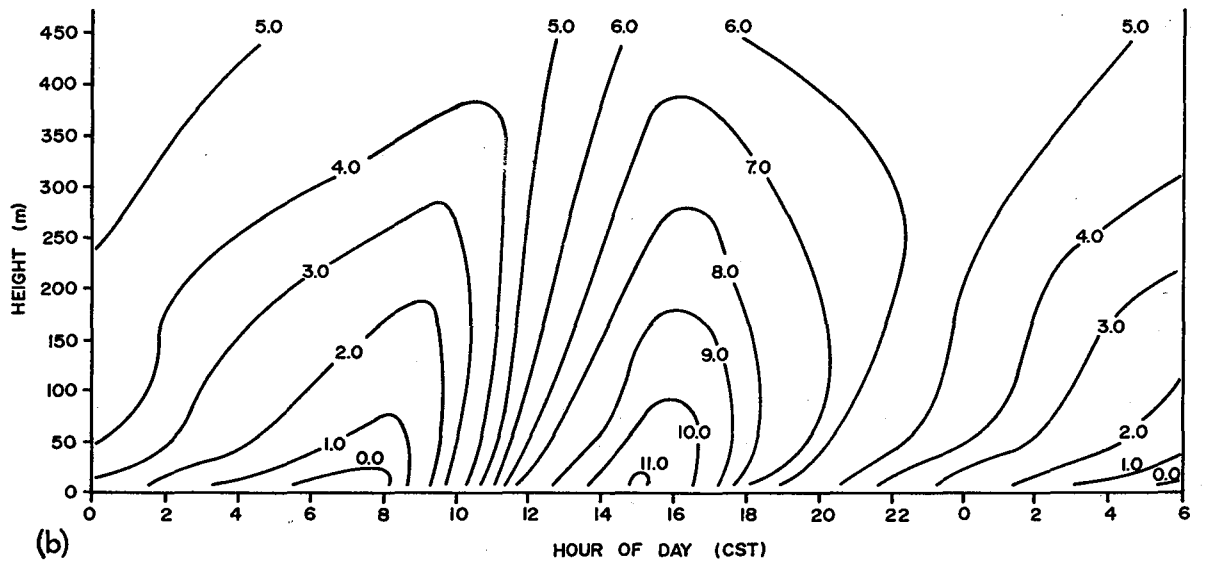
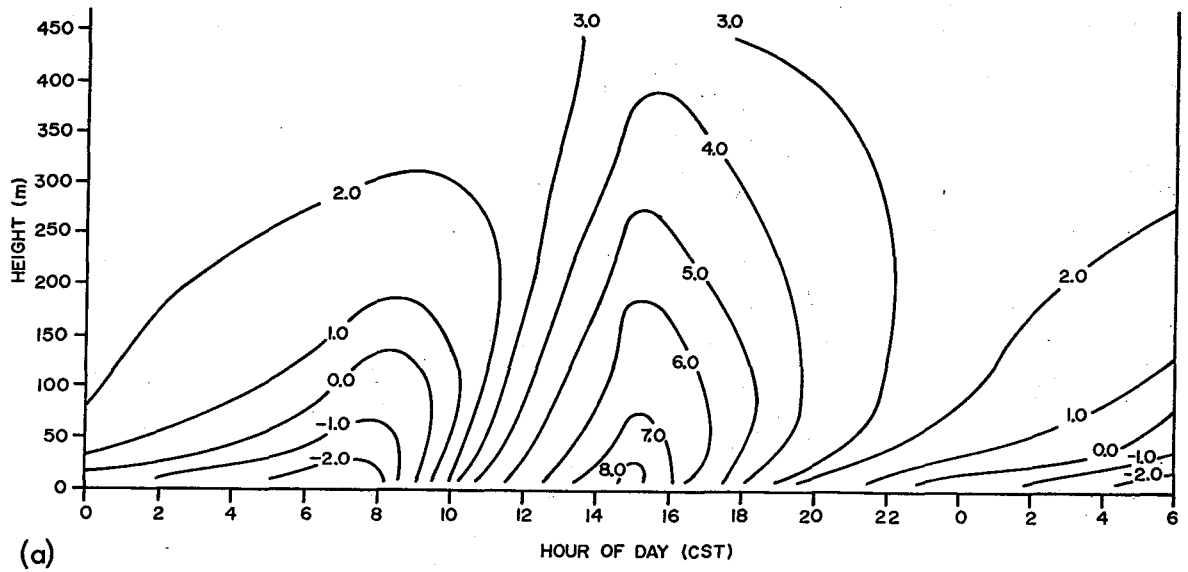


Figure 3a-b. Mean hourly temperatures ($^{\circ}\text{C}$): (a) December 1966, (b) January 1967.

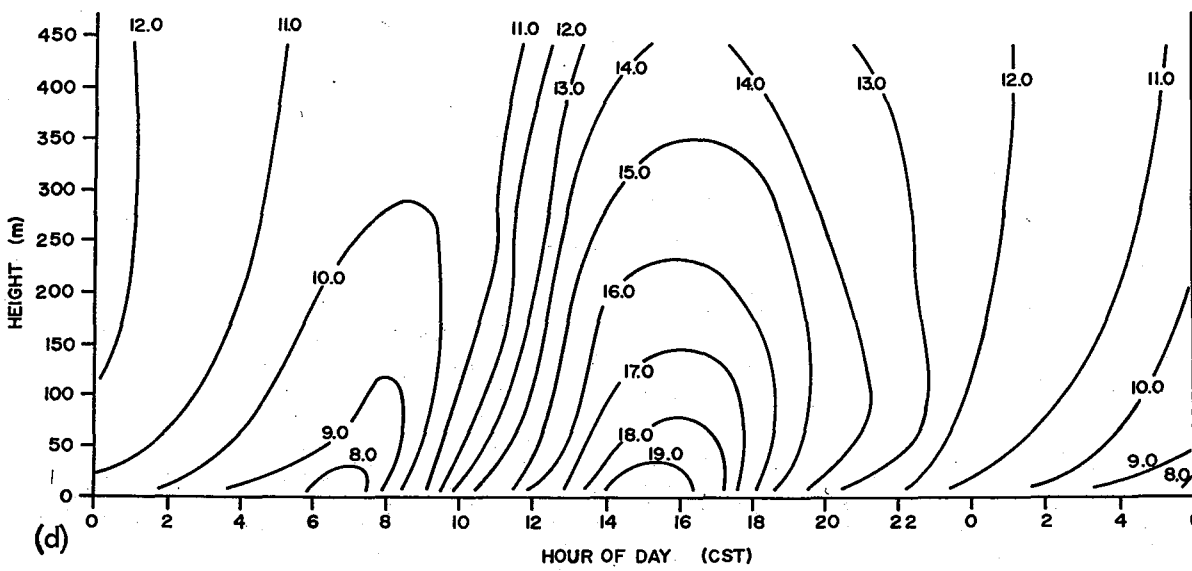
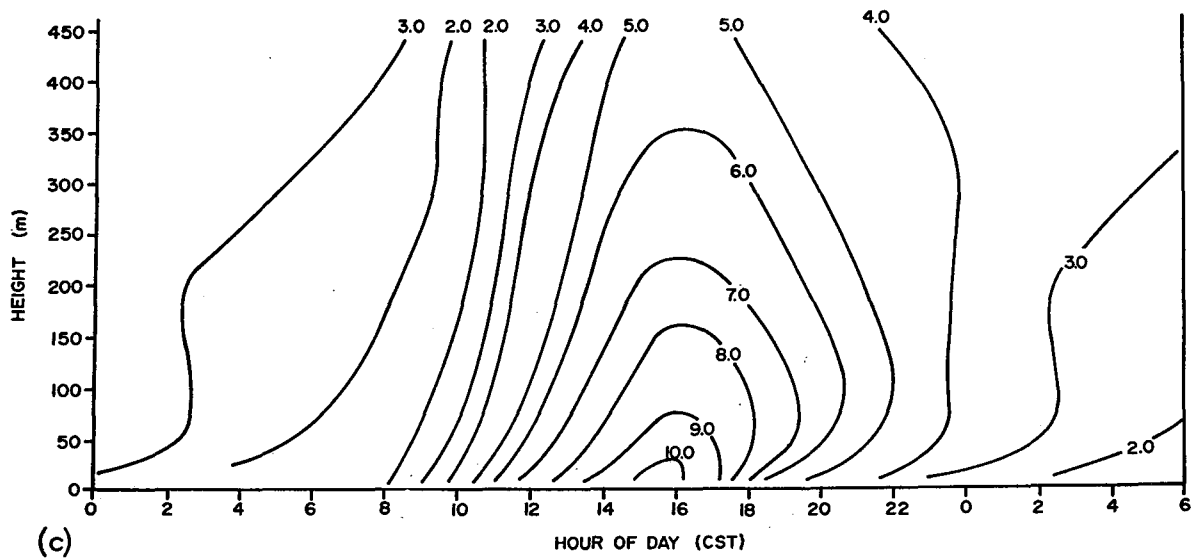


Figure 3c-d. Mean hourly temperatures (°C): (c) February 1967, (d) March 1967.

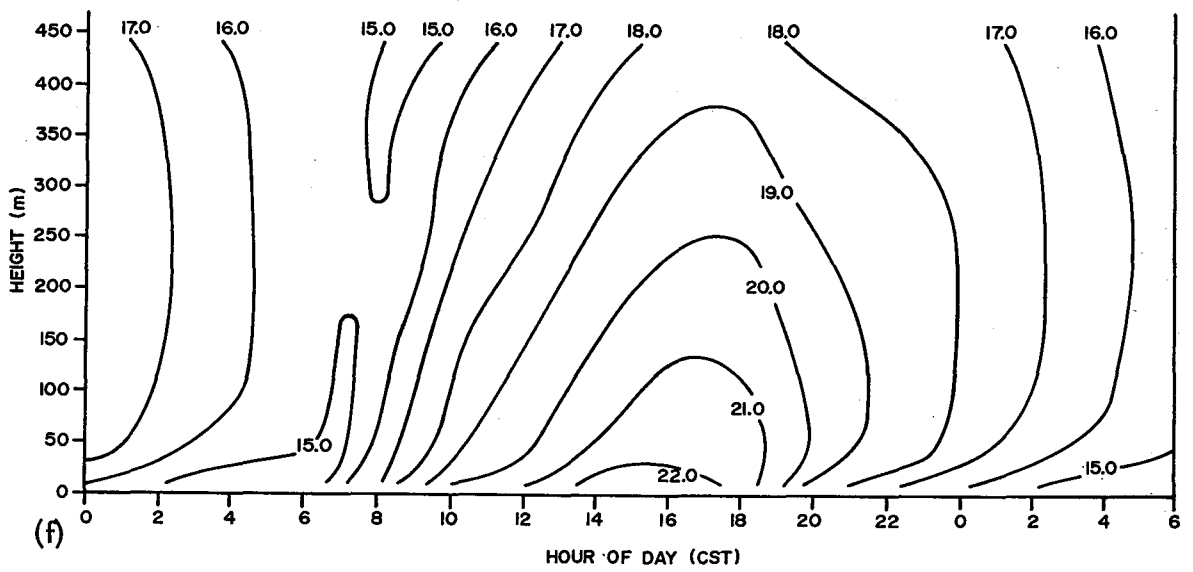
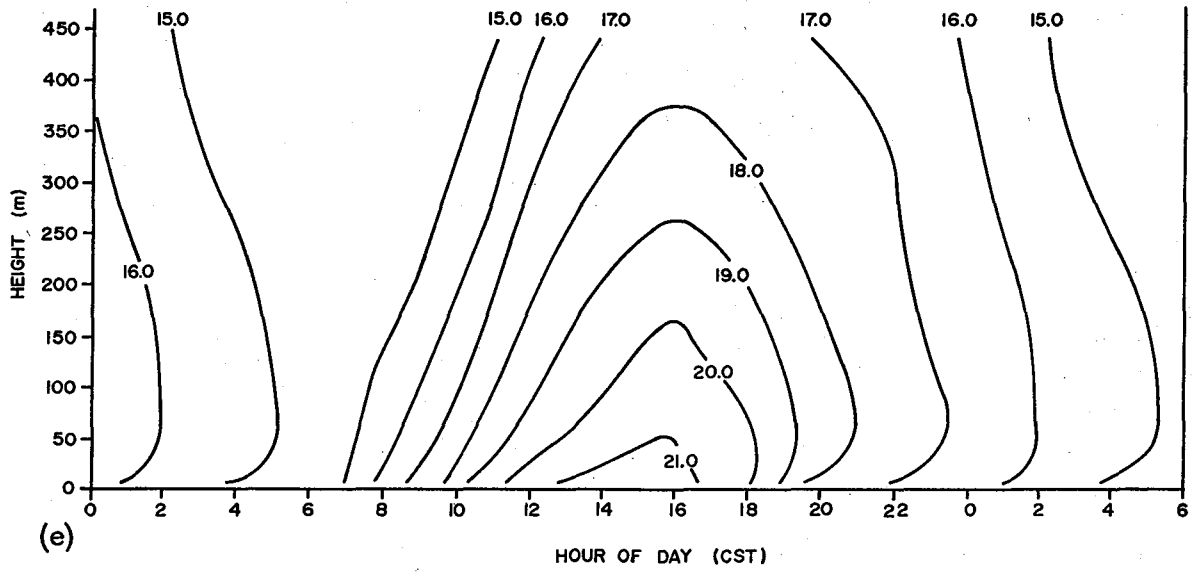


Figure 3e-f. Mean hourly temperatures ($^{\circ}\text{C}$): (e) April 1967, (f) May 1967.

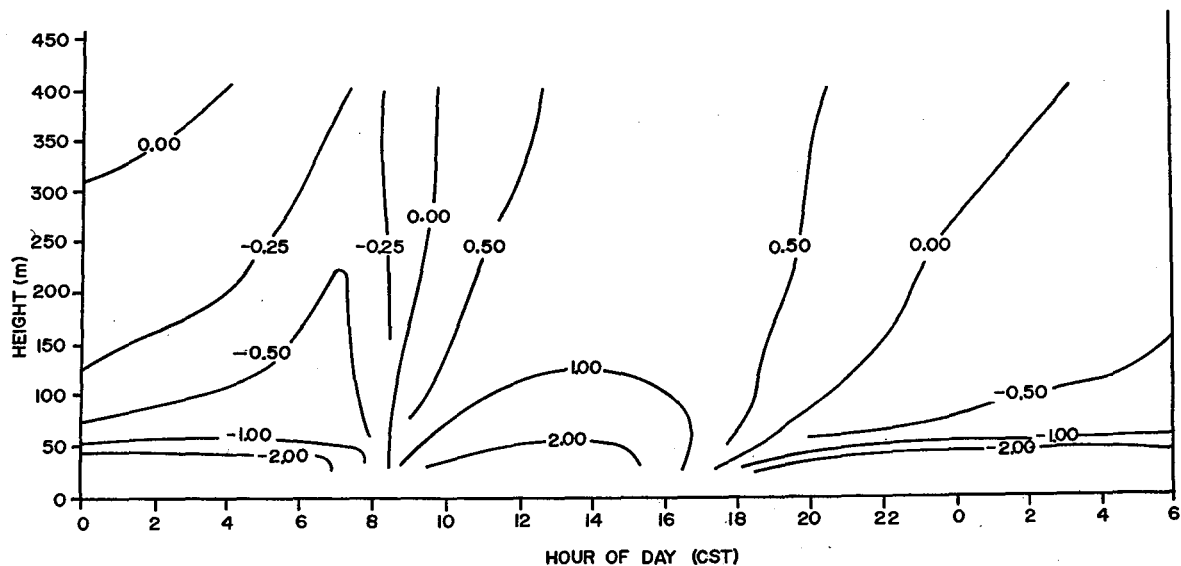


Figure 4. Mean hourly lapse rates ($-\partial T/\partial Z$ in $^{\circ}\text{C } 100 \text{ m}^{-1}$) for the whole sample.

convective mixing process spreads heat over a larger vertical extent and only a small amount is contributed to a given height. Heating above the surface lags the initial heating at the surface and the lag is a function of height. At 444 m the mean time lag is about 3 hrs (fig. 2), but varies from month to month (see figs. 3a-f). Gol'tsberg (1967) reports time differentials of 2 hrs in the warm season and 4 hrs in the cold season. His data are taken from the work of Selitskaya (1962) at Voeikova, U.S.S.R.

Maximum temperatures occur a few hours after local noon. Again, there is some lag with height, but the lag is considerably less than that of minimum temperatures. The 6 month mean chart (fig. 2) shows a lag of about 1 hr. and there is little difference from month to month (figs. 3a-f) except in June when the lag increases to 2 hrs. Johnson and Heywood (1938) observed a 45 min lag in the 1 to 87 m layer in December and a 1 hr and 25 min lag in June. Their results were obtained in England.

4. GENERAL LAPSE RATE CHARACTERISTICS

4.1 Hourly Means and Frequency Distributions

Hourly mean lapse rates (fig. 4) were calculated for the 6 month record and, as before⁴, data from all levels were omitted from the computation if a temperature

⁴ Lapse rates $-\partial T/\partial Z$, were computed by determining the temperature difference per 100 m between two levels. The same definition is used throughout this report.

at any level was missing. The most stable mean lapse rate at 23 m occurs at 0000, at 67 m at 0500, and at 400 m at 0800. Mean heights will be given when discussing lapse rates. It appears that there is a systematic vertical growth of the inversion throughout the night, but this is only partly true. Low-level inversions only grow to average heights of 150 to 200 m in mid-latitudes (Gol'tsberg, 1967), possibly higher in high latitudes and desert regimes. Highly stable lapse rates above 200 m after sunrise are the result of convectively induced lifting of surface inversions. This is discussed in more detail in Section 6.3.

Stability increases with height (fig. 4) during daylight hours. The sign of the lapse rate often does not change to positive until 1200 near the top of the tower. In the mean this occurs much earlier, however. A late morning transition time from the nighttime inversion condition implies a time no earlier than midday when the boundary layer and the free atmosphere are coupled.

Maximum positive lapse rates occur before the maximum temperature at all levels. The daily variation of positive lapse rate is closely tied to incoming solar radiation. Even though the lapse rate begins to decrease in the early afternoon, heating and vertical transport processes continue until the lapse rate is suppressed below gravitational convection rates.

The evening transition period⁵ begins with rapid cooling at low levels, and reversal of the sign of the lapse rate. The time of this sign change with respect to sunset varies little throughout the year (Best, 1935). Best found that the evening transition began about 1.5 hrs prior to sunset in the 30-120 cm layer. In the semi-desert, it starts 30 min later and in mountain valleys may start as much as 1.5 hrs after sunset (Gol'tsberg, 1967). Flower (1937) found a great variability in evening transition times in Egypt; however, events during the transition time are strongly influenced by the sky condition. Additional remarks on this subject, and subject of the upper level thermal structure during the transition time are given in the next section.

The frequency distributions of lapse rate for six layers are illustrated in figure 5a-f. Intervals of $0.25^{\circ}\text{C } 100 \text{ m}^{-1}$ were used in the main portion of the diagram. The inset shows the distribution near the dry adiabat in $0.05^{\circ}\text{C } 100 \text{ m}^{-1}$ intervals. The arrows indicate the dry adiabatic lapse rate. The range of lapse rates is large near the surface and decreases with height. At 23 m very strong inversions ($\partial T/\partial Z = +15.5^{\circ}\text{C } 100 \text{ m}^{-1}$) and very unstable gradients ($\partial T/\partial Z = -8^{\circ}\text{C } 100 \text{ m}^{-1}$) were observed in the 6 month record. These are by no means the extremes observed elsewhere. Records of the mean gradient at Porton, England (Best, 1935) indicate that

⁵ Transition periods occur after sunrise or sunset when the boundary layer is adjusting to the addition of or loss of radiant energy. The transition period after sunrise is most conspicuous.

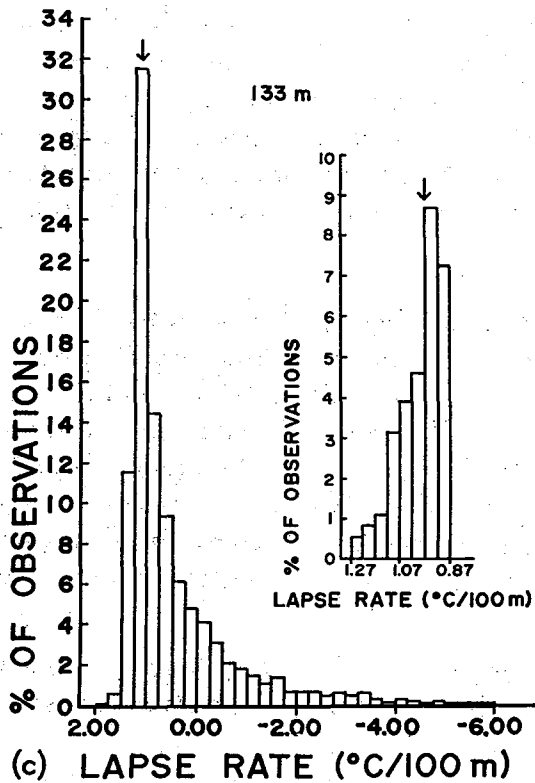
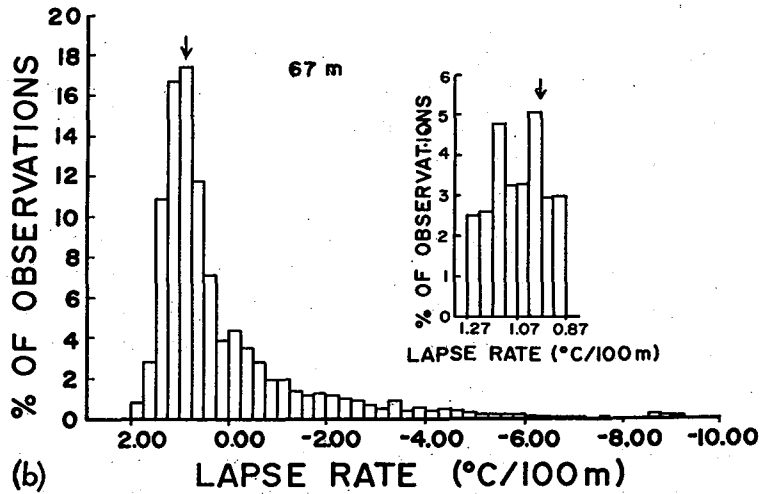
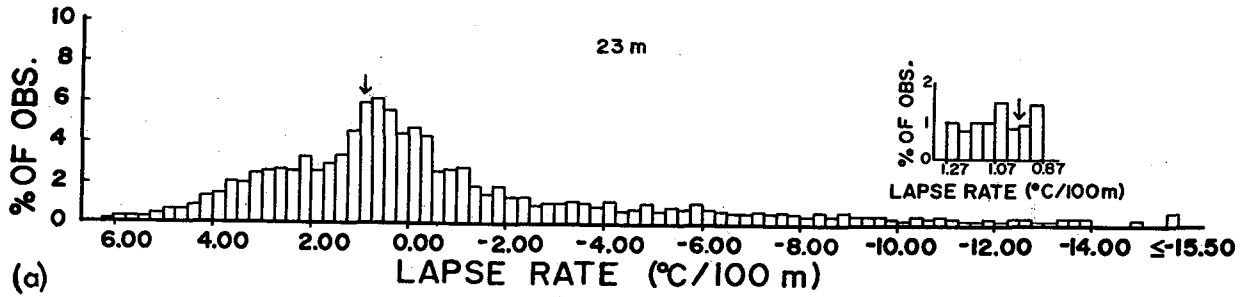


Figure 5a-c. Relative frequency distribution of lapse rate ($^{\circ}\text{C } 100\text{ m}^{-1}$). Inserts give greater resolution around the dry adiabat (arrows): (a) 23 m, (b) 67 m, (c) 133 m.

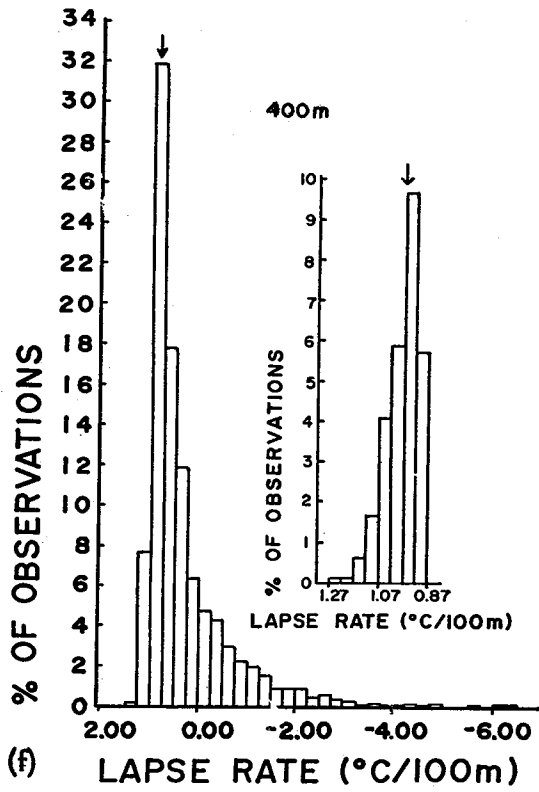
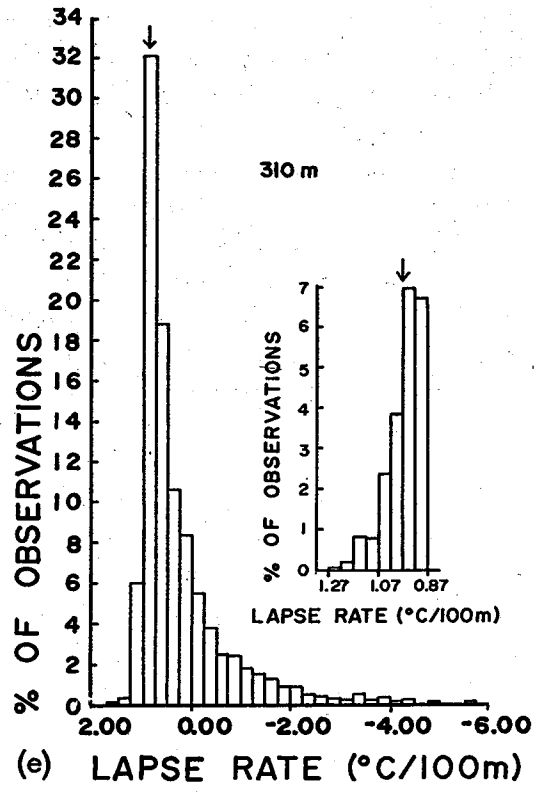
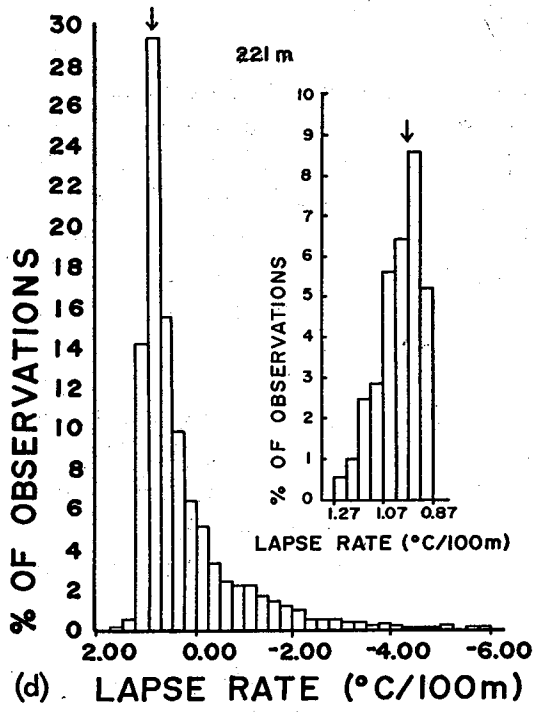


Figure 5d-f. Relative frequency distribution of lapse rate ($^{\circ}\text{C } 100 \text{ m}^{-1}$). Inserts give greater resolution around the dry adiabats (arrows): (d) 221 m, (e) 310 m, (f) 400 m.

occasional very strong gradients are possible near the ground. Both stable and unstable gradients exceeding 1000 multiples of the dry adiabatic lapse rate were observed in the 2.5 to 30 cm layer at Porton.

For levels above 100 m, the ranges and distributions of the lapse rate are quite similar. Each distribution is clustered around the dry adiabatic value, falling off rapidly for more stable and unstable lapse rates. Separate analysis of cloudless daytime observations indicates that the dry adiabat constitutes an upper limit for the lapse rate. Below 100 m, in the superadiabatic layer, this is not the case. The 100 m value seems to be the approximate depth necessary for the atmosphere to adjust from the strongly heated surface layer with a large thermal gradient to near neutral conditions.

Best, et al. (1952) observed in England that 92 percent of all lapse rates at a mean height of 76 m were below the dry adiabatic lapse rate. Brocks (1948) has plotted many measurements of the lapse in Europe and Egypt in one diagram. He shows the mean depth of the unstable layer to be about 10 m in December and 60 m in June. These values are much lower than those determined for central Oklahoma - especially for the winter case.

Crude estimates of the depth of the unstable layer can be inferred from Table 2, also. More significant, however, are the figures for stability. Table 2 demonstrates that inversions in general (i.e., the moderately stable case) are uniformly distributed in the lowest 450 m, although the table does not relate the inversion distribution to factors responsible for its character.

Table 2. Frequency Distribution of Lapse Rate ($^{\circ}\text{C } 100 \text{ m}^{-1}$) for Six Layers and Four Stability Groups.

| Mean Height (m) | SS | MS | WS | U |
|-----------------|------|------|------|------|
| 400 | 1.0 | 23.1 | 68.0 | 7.9 |
| 310 | 0.7 | 22.9 | 69.9 | 6.5 |
| 221 | 1.0 | 23.2 | 61.1 | 14.7 |
| 133 | 3.8 | 22.8 | 61.1 | 12.3 |
| 67 | 3.8 | 24.7 | 40.2 | 31.3 |
| 23 | 16.4 | 28.3 | 21.4 | 33.9 |

| | | |
|---------|------------------------|----------------------------------------------------------|
| Legend: | Strongly stable (SS) | $\delta \leq -4^{\circ}\text{C } 100 \text{ m}^{-1}$ |
| | Moderately stable (MS) | $0 \geq \delta > -4^{\circ}\text{C } 100 \text{ m}^{-1}$ |
| | Weakly stable (WS) | $1 \geq \delta > 0^{\circ}\text{C } 100 \text{ m}^{-1}$ |
| | Unstable (U) | $\delta > 1^{\circ}\text{C } 100 \text{ m}^{-1}$ |

It will be seen that certain atmospheric processes such as radiation, advection, and subsidence are more influential in some portions of the boundary layer than others. For example, long wave radiation is known to be the principal cause of low level inversions, producing stronger inversions than any other source. Table 2 indicates that intense inversions are confined to the lowest levels (below 50 m) and are extremely rare above 200 m. We may, therefore, conclude that long wave radiation is important below 50 m and becomes less insignificant at higher levels including the free atmosphere (Staley and Jurica, 1968).

4.2 Characteristics of Time Adjusted Data

In the previous section, the relationship between thermal gradients and spatial (vertical) and temporal change were discussed. This type of presentation allowed easy comparison to other similar investigations, but glossed over the significant events that might occur during the sunrise and sunset transition periods. The importance of this becomes obvious when one considers the annual variation in the time of local sunrise and sunset (> 2 hrs in Oklahoma). Further, there has been little prior mention in this report of the effect of cloud cover on the boundary layer temperature gradient, a factor known to be important (Haurwitz and Austin, 1944). Last, antecedent literature is scanty regarding the character of the lapse rate in the tower layer in different air masses.

To combine the meteorological criteria in an analysis of the mean lapse rate near the transition period, daily records were first adjusted to hourly intervals before and after sunset, then averaged according to general sky conditions in different air masses.⁶

Mean lapse rate data adjusted to the local sunset time are illustrated in figures 6a-g. The mean heights of the three layers indicated are 67 m (layer 2), 221 m (layer 4) and 400 m (layer 6). Air mass data were derived from the Daily Weather Map Series (U.S. Dept. of Commerce, 1966-7), and sky conditions were determined from Oklahoma City Weather Bureau (NWS) observations.⁷ Cloudy conditions include overcast low and/or middle cloud cover and surface obscuration in fog.

The general characteristics of the lapse rate for the six month sample are shown in figure 6a. Earlier results indicated that there was little time variation in the maximum diurnal lapse rate from the surface to 400 m. When data are adjusted to local

⁶ For example, when the sunrise is at 0710, the observation for 0700 is considered to be made at sunrise, and the observation for 0800 is considered to be made 1 hr after sunrise.

⁷ There is no figure for cloudy mT, clear cT and cloudy cT air masses since the sample sizes were too small for statistical evaluation. Partly cloudy air masses which constitute a small portion of the sample were not analyzed.

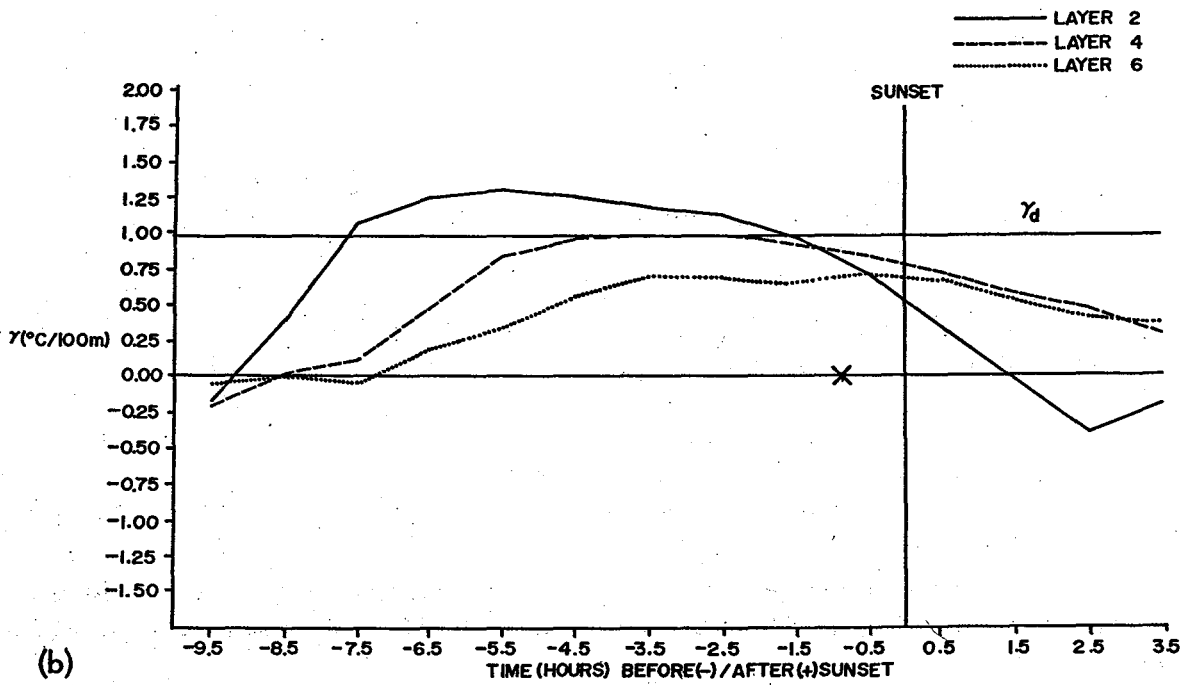
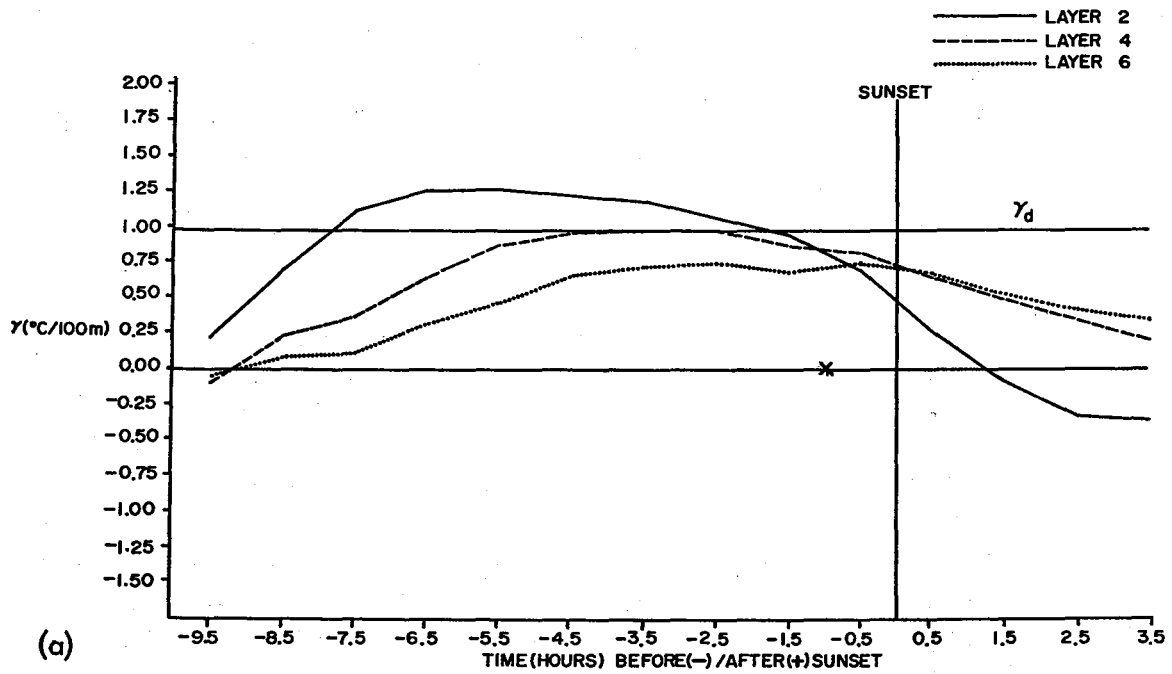


Figure 6a-b. Lapse rate ($^{\circ}\text{C } 100 \text{ m}^{-1}$) versus time before/after sunset; (a) Whole sample, (b) cP air masses.

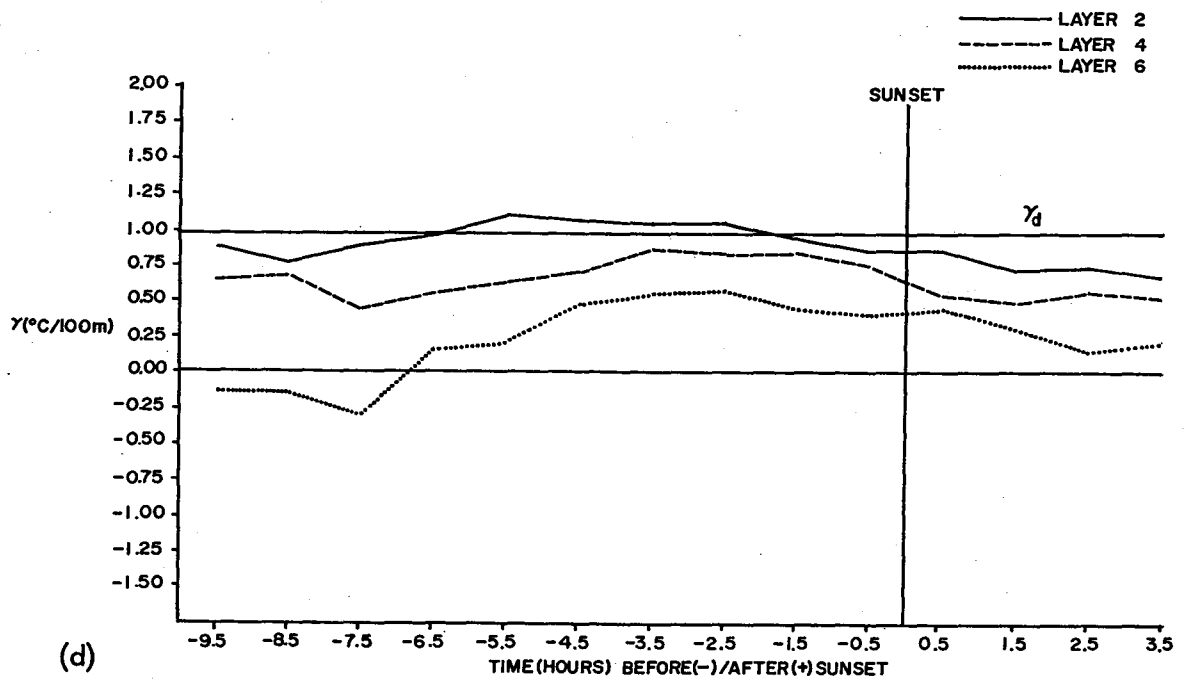
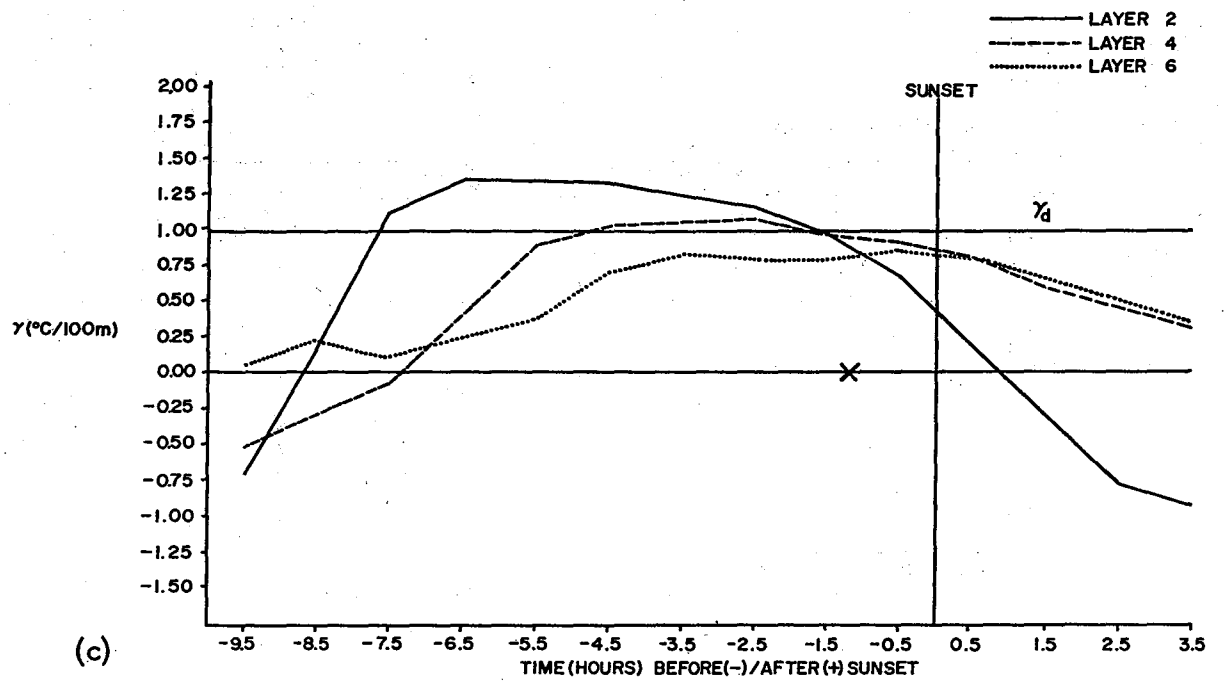


Figure 6c-d. Lapse rate ($^{\circ}\text{C } 100 \text{ m}^{-1}$) versus time before/after sunset: (c) Clear cP air masses, (d) Cloudy cP air masses.

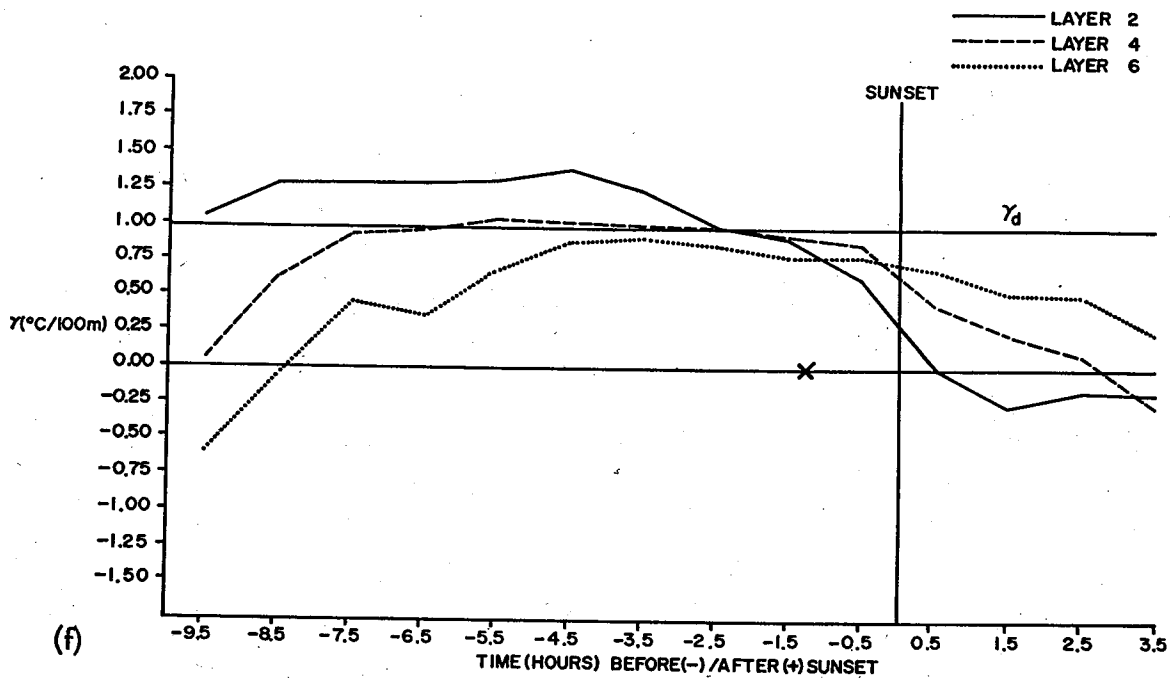
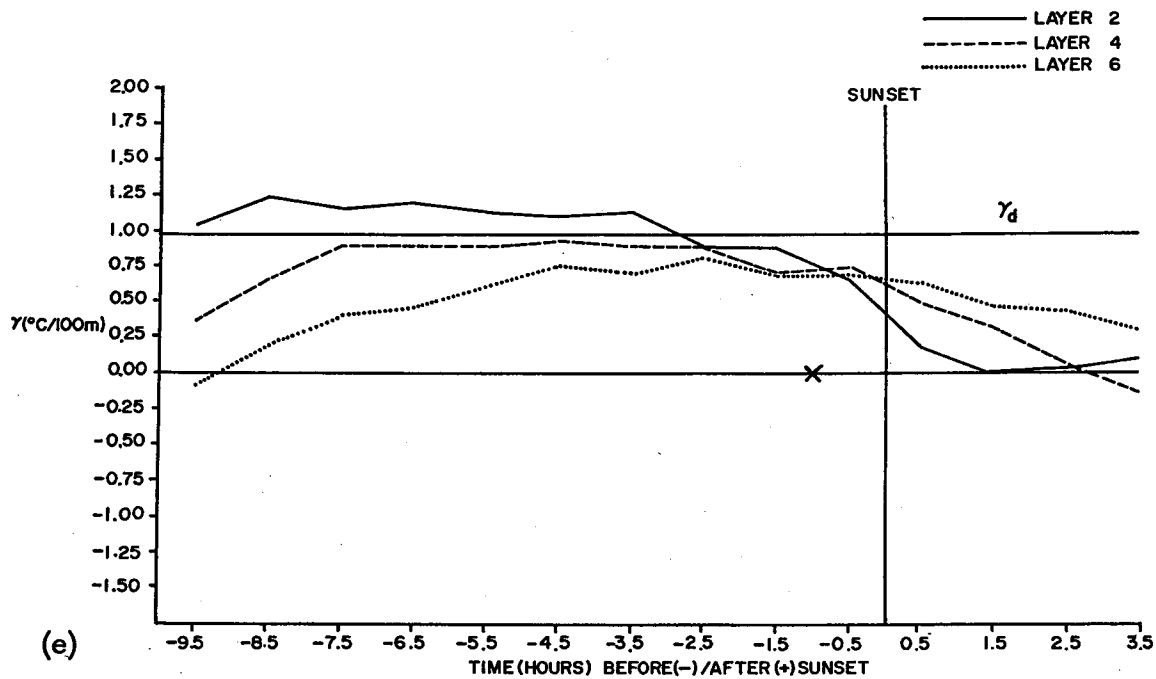


Figure 6e-f. Lapse rate ($^{\circ}\text{C } 100 \text{ m}^{-1}$) versus time before/after sunset: (e) All mT air masses, (f) Clear mT air masses.

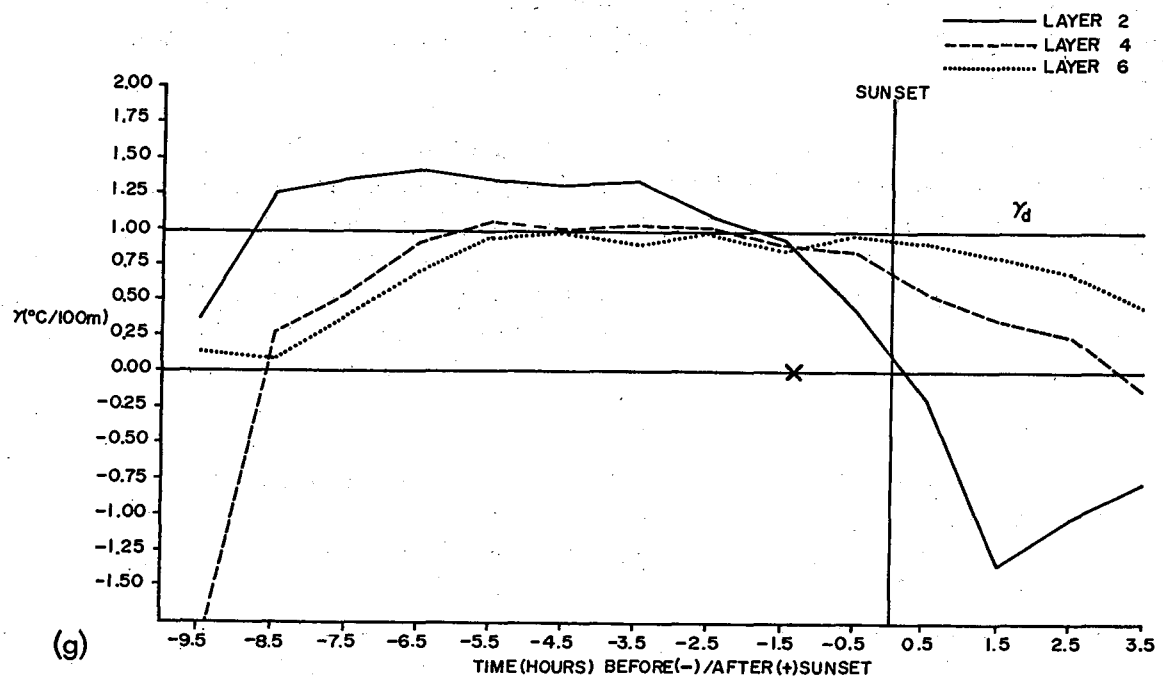


Figure 6g. Lapse rate ($^{\circ}\text{C } 100 \text{ m}^{-1}$) versus time before/after sunset: (g) cT air masses.

sunset, however, there is often a lag of many hours. The time shift is about 4 hrs for the 6 month record. When data are separated by air mass and sky condition, the lag is still evident (figs. 6b-g). Such is the case in continental polar (cP) air masses for all types of cloud cover and clear polar air masses. In the continental tropical (cT) air mass⁸, the lag is difficult to determine since the 400 m lapse rate remains nearly neutral for many hours in the afternoon. The situation is also nebulous in the maritime (mT) air mass and cloudy polar air masses.

Inversions form quickly near sunset at low levels, except when there is cloud cover (fig. 6d). The curve for layer 2 (67 m) indicates that isothermal conditions are reached 0.5 to 1.5 hrs after sunset. The curve for 23 m is not plotted, but the "x" shown on the isothermal line specifies the time of inversion formation at 23 m

⁸Continental tropical air masses are specifically defined here as dried and warmed maritime polar air masses that have lost their original characteristics in traversing the Rocky Mountains. True cT air masses, as defined by Bergeron (Berry, Bollay and Beers, 1945), originating over the Central Mexican Plateau or in the southwestern United States are also included in this group. Also included in this group is the extremely dry Superior air mass.

(if this condition is reached). The fact that inversions form before sunset substantiates earlier results in this report and agrees with most prior investigations (Geiger, 1965).

Inversions seem to rapidly intensify after sunset, then suddenly become weaker. Radiational cooling occurs near the surface first, and its effects gradually penetrate a deeper layer. For two widely spaced instruments, only the bottom level responds to the rapid cooling at first. As the inversion deepens, the top level eventually responds to the rapid cooling; however, by the time the top instrument responds, the rate of cooling has diminished at the lower instrument, effectively weakening the inversion. Thus, the rate of cooling may be thought of as a vertically propagating wave.

Maritime air masses exhibit a nighttime thermal structure somewhat different than other air masses. About 3 hrs after sunset, the 221 m layer has a tendency to become more stable than the lower layer. The cause of this mid-boundary layer stability is probably not radiation, since radiation is more important near the surface. The evidence presented so far is insufficient to make further comment. Additional comments will be made in section 5.2 where a more detailed analysis is made of this air mass and its vertical temperature structure.

General lapse rate characteristics in the tower layer do not appear to differ markedly between air masses especially during the day, but are more strongly a function of the cloud cover. This statement may not hold in regions with climates different from Oklahoma, and further investigation is necessary.

There appears to be a consistent secondary peak in the 400 m lapse rate near sunset (figs. 6a-g) with a minimum in the late afternoon. In the case of the clear cP air masses (fig. 6c) the peak near sunset is the primary peak. This has apparently weighted the mean lapse rates for all cP air masses (fig. 6b) so that a primary peak near sunset for this air mass condition is also evident at 400 m.

Figure 7 indicates the percentage of observations that exceed the dry adiabatic lapse rate for 67, 221, and 400 m (layers 2, 4 and 6, respectively) adjusted to the sunset times as before. The secondary maximum at 400 m is now more obvious. Several cases which exhibited this secondary peak were investigated. The event appeared to be more frequent in the winter months than in the spring and in clear, dry air masses rather than overcast, moist air masses. Continental polar air masses are frequent in the winter, and we may speculate that this phenomenon is more apt to occur in air masses with moisture characteristics similar to those of the continental polar air mass. This includes the continental tropical air mass which is always relatively dry and usually cloud-free. Continental polar air masses are not always cloud-free, however (fig. 6d).

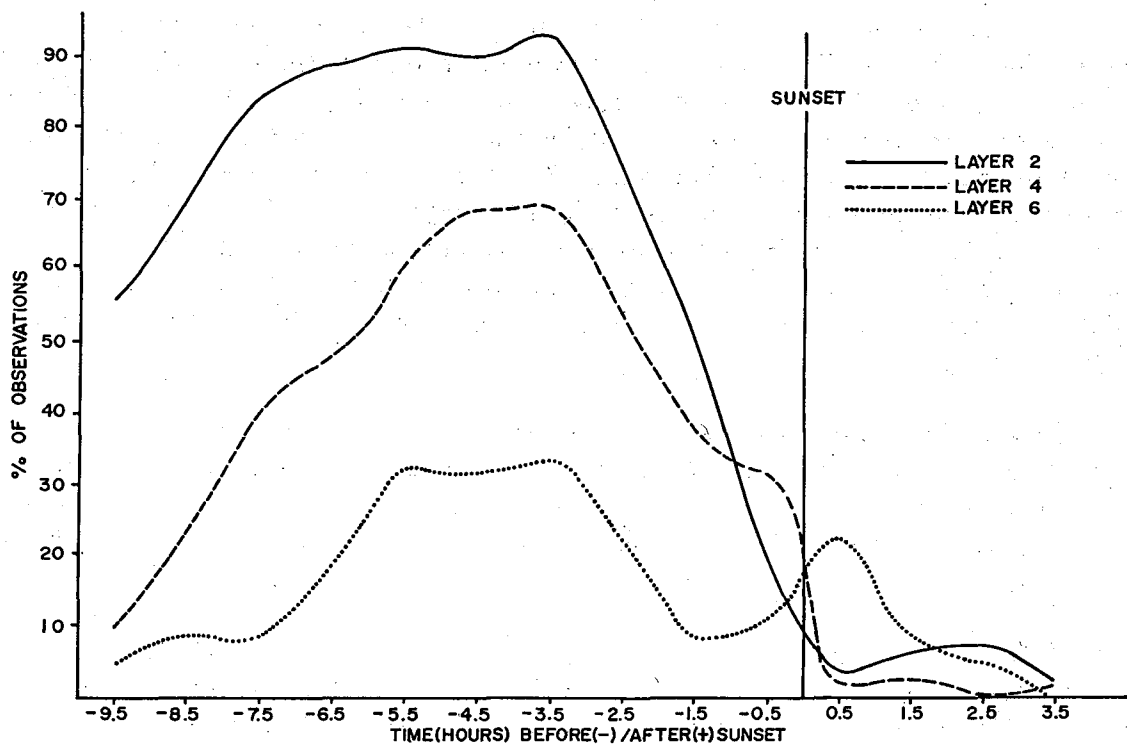


Figure 7. Relative frequency of $\gamma \geq \gamma_d$ versus time before/after sunset.

In clear, dry continental polar and continental tropical air masses, diurnal heating and cooling is strong and occurs in a deep layer near the surface (see also section 5.2). Near sunset a rapid loss of heat and resulting vertical shrinkage of the lowest layer may cause subsidence aloft. Vertical mass convergence in the free atmosphere has been illustrated by Saucier (1953). In an atmosphere that is absolutely stable near the surface, conditionally stable in the mid-boundary layer and neutral in the upper portions of the boundary layer, subsidence results in an effective lowering of the base of the neutral layer into a region that was formerly conditionally stable. For example, this causes the rate of $\partial T / \partial t$ (the second derivation with respect to time) at 355 m (the top of the conditionally stable layer) to decrease while having little effect on the rate of $\partial T / \partial t$ at 444 m, a tendency toward instability.

The above explanation is speculative. There is no information about the behavior of, or the initial (pre-sunset) conditions of, the atmosphere above 450 m; and the spacing of the data does not allow us to confirm such subtle changes in the atmosphere. The event appears to be short-lived.

The mean depth of the well-mixed surface layer can be inferred from figures 6a-g. The term "well-mixed" is defined as that thermal stratification in which $\gamma \geq \gamma_d$, where γ is the ambient lapse rate. Table 3 gives subjectively determined values of the mean depth of the different air mass classifications obtained from these figures. The table should only be used as a general comparison of air masses. It shows that under clear conditions the mean depth of the well-mixed layer is nearly the depth of the tower layer. Under certain conditions, however, the depth of the well-mixed layer may be much greater than 450 m. There is much greater variation of the depth due to changes in the sky condition than to changes in the air mass.

Figures 8a-g are similar to figures 6a-g, except that the data have been adjusted to the sunrise times. In figure 8a pre-sunrise inversions are strongest in the lowest layers. Maximum intensities occur 1.5 hrs prior to sunrise at 23 m but 0.5 hrs after sunrise at 221 and 400 m. At 400 m, inversions persist up to 3.5 hrs after sunrise.

Shortly after sunrise the transition period begins, indicated in figure 8a by points A1, A2, and A3 for 67, 221, and 400 m, respectively. After initiation of the transition period near the surface, there is a considerable time lag of initiation at higher levels: 2.5 hrs after sunrise at 400 m (layer 6). The length of the transition period also varies with height. It is 2 hrs long at 67 m, and 3 hrs long at the top of the tower; therefore, the boundary layer and the free atmosphere are not coupled until 5.5 hrs after sunrise or around 1200. The end of the transition period for each of the three layers is denoted in figure 8a by points B1, B2, and B3. The points denoting the beginning and ending of the transition times are not shown in figures 8b-g, but can easily be deduced by the reader. There is obviously no transition period for the cloudy cP air mass condition (fig. 8d).

Table 3. Mean Depth of the Well-Mixed Layer

| Air Mass Code | Depth (m) (approx. values) |
|---------------|-------------------------------|
| Whole sample | 250 |
| cP | 275 |
| Clear cP | 325 |
| Cloudy cP | 150 |
| mT | 225 |
| Clear mT | 350 |
| cT | 450 |

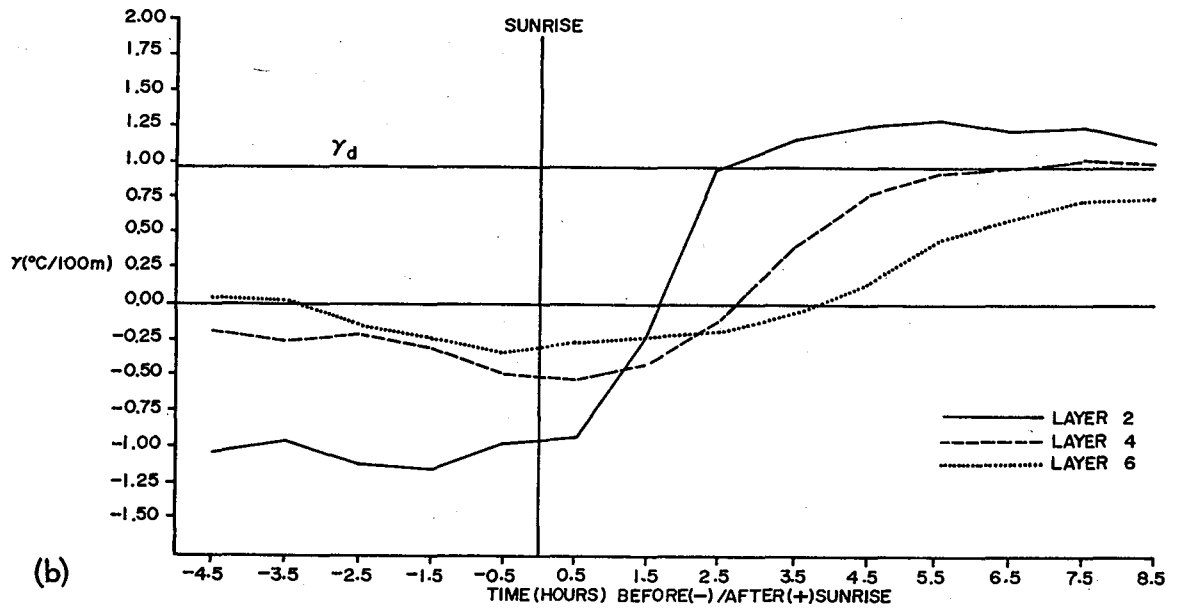
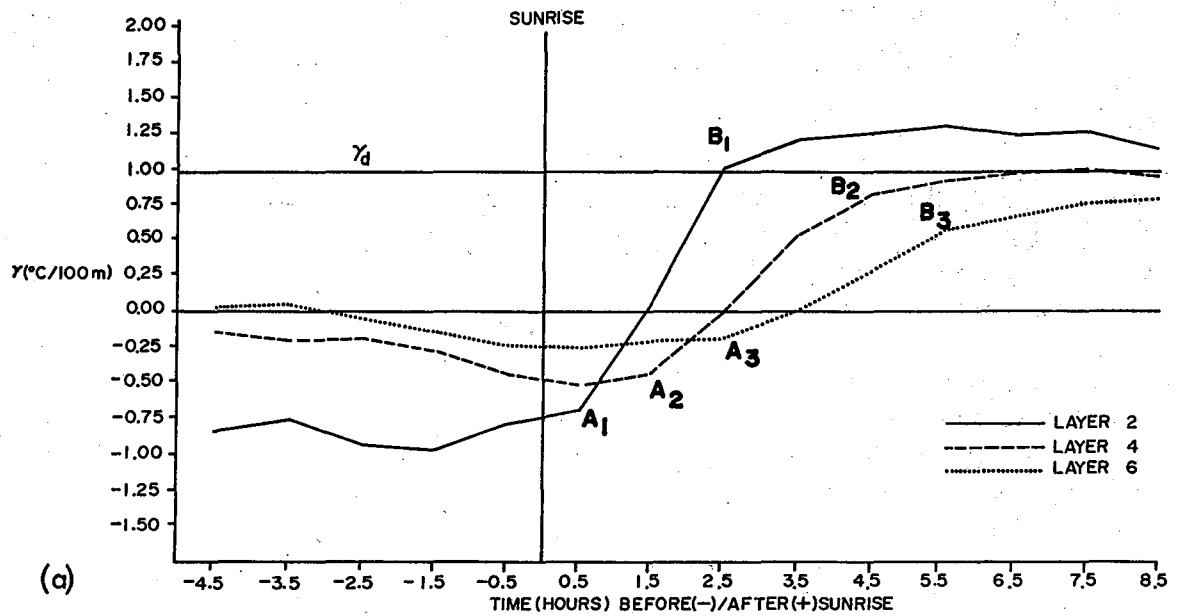


Figure 8a-b. Lapse rate ($^{\circ}\text{C } 100 \text{ m}^{-1}$) versus time before/after sunrise: (a) Whole sample, (b) cP air masses.

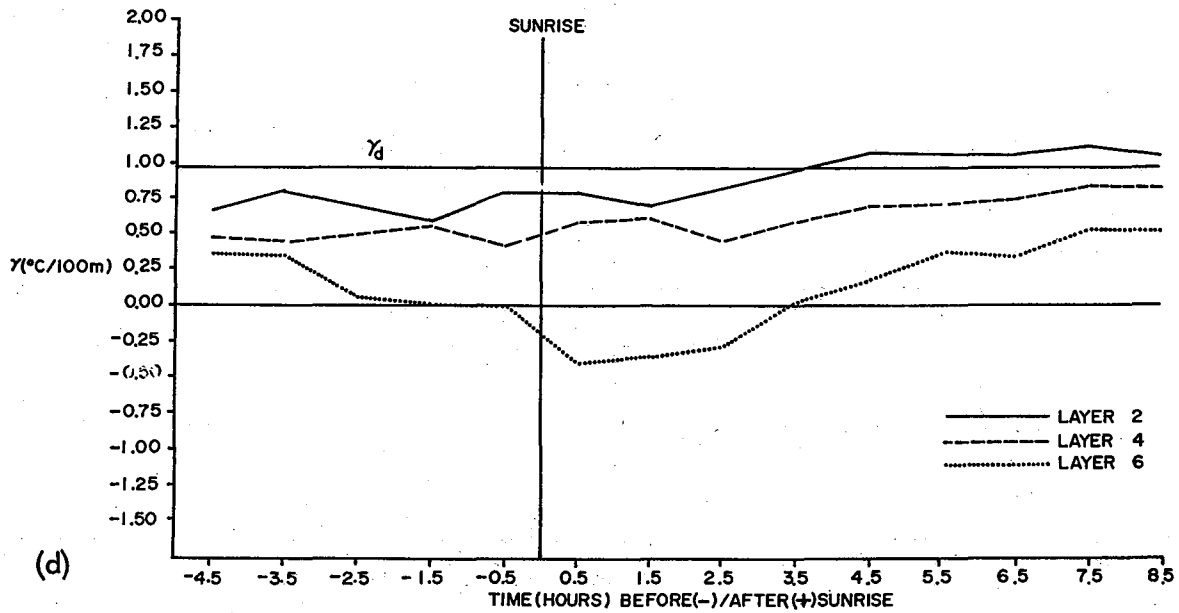
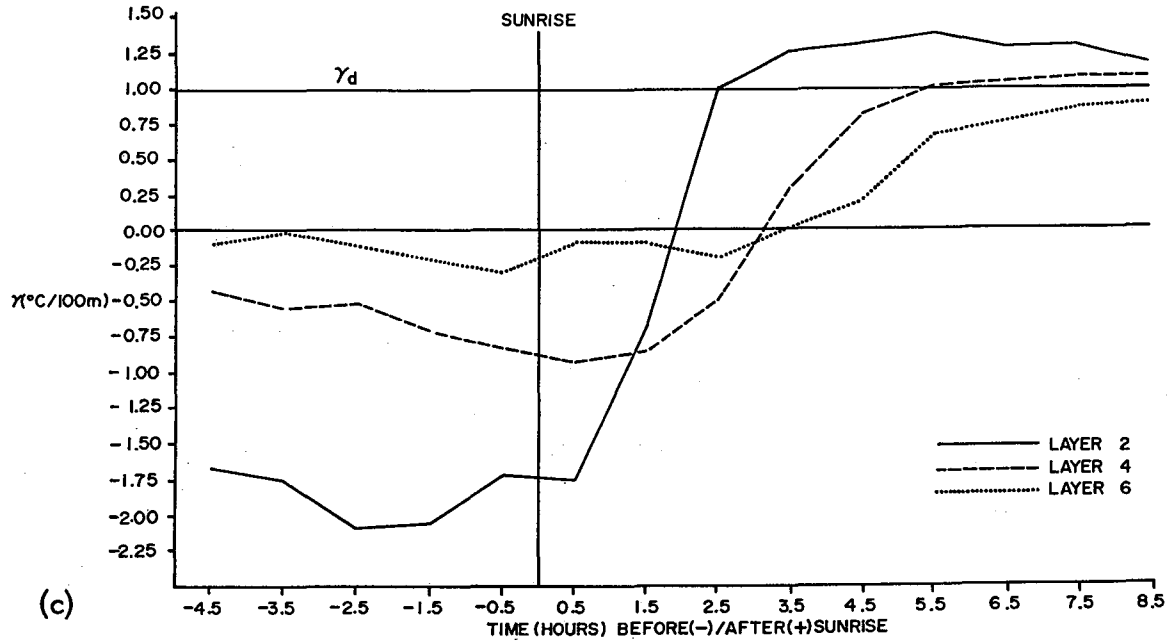


Figure 8c-d. Lapse rate ($^{\circ}\text{C } 100 \text{ m}^{-1}$) versus time before/after sunrise: (c) Clear cP air masses, (d) Cloudy cP air masses.

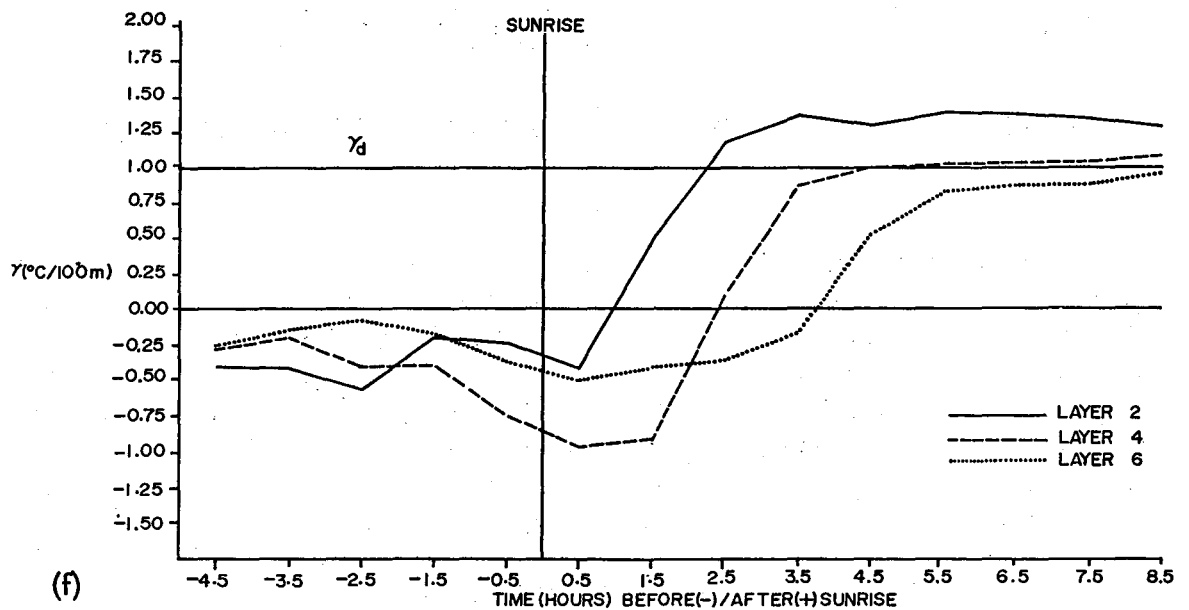
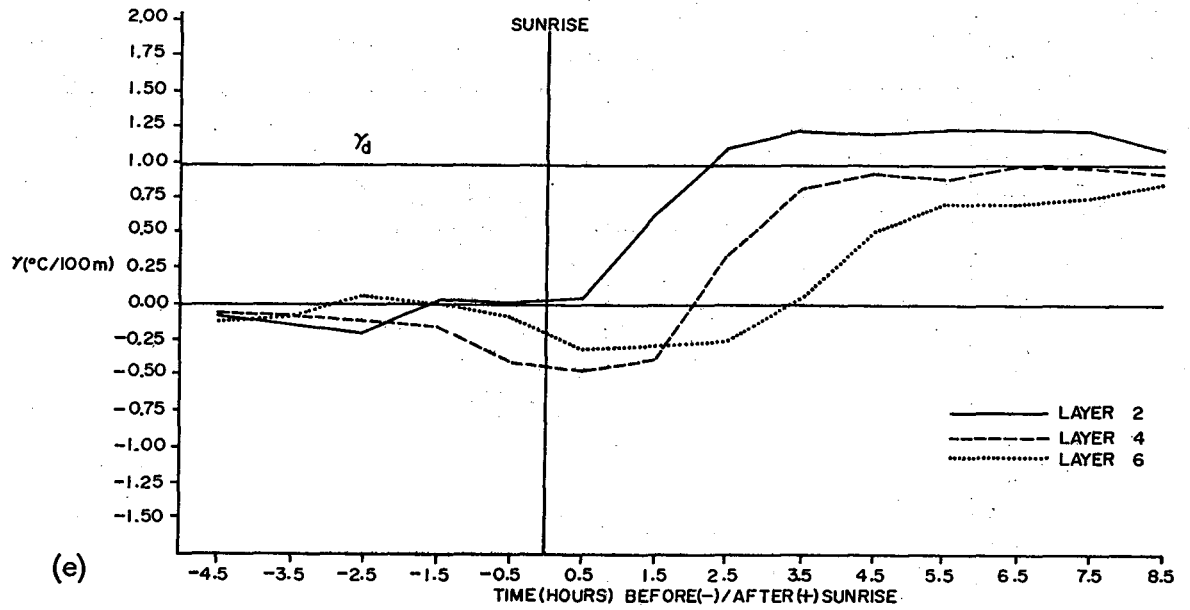


Figure 8e-f. Lapse rate ($^{\circ}\text{C } 100 \text{ m}^{-1}$) versus time before/after sunrise: (e) mT air masses, (f) Clear mT air masses.

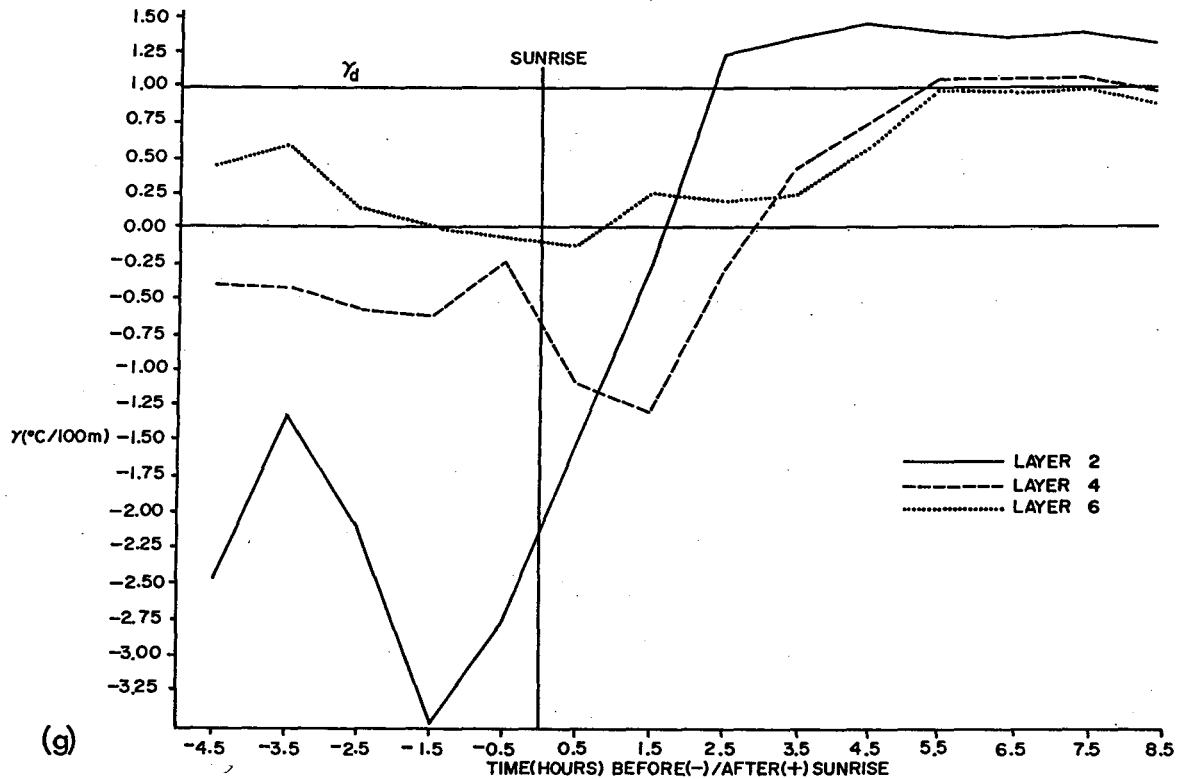


Figure 8g. Lapse rate ($^{\circ}\text{C } 100 \text{ m}^{-1}$) versus time before/after sunset: (g) cT air masses.

The remaining figures in this group show the variations for different air mass and cloud cover classifications. The behavior of cP air masses and clear cP air masses (figs. 8b and 8c) is much the same as for the whole sample, except that inversions prior to sunrise are stronger in the case of the latter, and the mid-day lapse rate is steeper. Maritime tropical air masses (fig. 8e) are different in that nocturnal inversions are weak in all layers but are most intense in the mid-levels just prior to sunrise. Continental tropical air masses are characterized by strong surface inversions at night and steep mid-day lapse rates throughout the tower layer.

4.3 Thermal Stratification Versus Wind Characteristics

For each layer, four stability groups (see table 2) were established and contingency tables of wind speed versus direction for the level at the bottom of the layer were determined. Data for the lowest and highest layers are shown in table 4.

Table 4. Probability of Wind Speed for Given Wind Direction at 23 and 400 m for Four Stability Groups.

| Wind Dir. | 23 m | | | | 400 m | | | | | | |
|-----------|------------------------------|-------------|-------------|-------------|------------------------------|-------------|-------------|-------------|-------------|-------------|--------------|
| | Speed (m sec ⁻¹) | | | | Speed (m sec ⁻¹) | | | | | | |
| | 0-5 | 5-10 | 10-15 | Total | 0-5 | 5-10 | 10-15 | 15-20 | 20-25 | Total | |
| SS | N | .166 | .002 | 0 | .168 | .070 | .047 | 0 | 0 | 0 | .117 |
| | E | .140 | 0 | 0 | .140 | .070 | .047 | .070 | 0 | 0 | .187 |
| | S | .460 | 0 | 0 | .460 | 0 | .116 | .116 | .302 | .023 | .557 |
| | W | .232 | 0 | 0 | .232 | .023 | .093 | 0 | .023 | 0 | .139 |
| | T | <u>.998</u> | <u>.002</u> | <u>0</u> | <u>1.000</u> | <u>.163</u> | <u>.303</u> | <u>.186</u> | <u>.325</u> | <u>.023</u> | <u>1.000</u> |
| MS | N | .175 | .026 | .001 | .202 | .067 | .084 | .033 | .002 | 0 | .186 |
| | E | .125 | .016 | .001 | .142 | .055 | .086 | .057 | .016 | .004 | .218 |
| | S | .304 | .260 | .008 | .572 | .032 | .070 | .102 | .121 | .131 | .456 |
| | W | <u>.072</u> | <u>.011</u> | <u>.001</u> | <u>.084</u> | <u>.038</u> | <u>.045</u> | <u>.029</u> | <u>.017</u> | <u>.011</u> | <u>.140</u> |
| | T | <u>.676</u> | <u>.313</u> | <u>.011</u> | <u>1.000</u> | <u>.192</u> | <u>.285</u> | <u>.221</u> | <u>.156</u> | <u>.146</u> | <u>1.000</u> |
| WS | N | .091 | .170 | .022 | .283 | .055 | .102 | .082 | .016 | 0 | .255 |
| | E | .101 | .048 | 0 | .149 | .037 | .065 | .020 | .002 | .001 | .125 |
| | S | .148 | .347 | .022 | .517 | .051 | .109 | .147 | .121 | .039 | .467 |
| | W | <u>.024</u> | <u>.025</u> | <u>.002</u> | <u>.051</u> | <u>.045</u> | <u>.050</u> | <u>.048</u> | <u>.009</u> | <u>.001</u> | <u>.153</u> |
| | T | <u>.364</u> | <u>.590</u> | <u>.046</u> | <u>1.000</u> | <u>.188</u> | <u>.326</u> | <u>.297</u> | <u>.148</u> | <u>.041</u> | <u>1.000</u> |
| U | N | .126 | .177 | .031 | .334 | .075 | .210 | .137 | .022 | 0 | .444 |
| | E | .096 | .044 | .001 | .141 | .057 | .065 | .003 | 0 | 0 | .125 |
| | S | .121 | .240 | .029 | .390 | .062 | .091 | .100 | .019 | .003 | .275 |
| | W | <u>.085</u> | <u>.046</u> | <u>.004</u> | <u>.135</u> | <u>.051</u> | <u>.065</u> | <u>.032</u> | <u>.008</u> | <u>0</u> | <u>.156</u> |
| | T | <u>.428</u> | <u>.507</u> | <u>.065</u> | <u>1.000</u> | <u>.245</u> | <u>.431</u> | <u>.272</u> | <u>.049</u> | <u>.003</u> | <u>1.000</u> |

Four direction intervals centered on 0° , 90° , 180° , and 270° and five speed intervals in m sec^{-1} ($0.1 - 5$, $5.1 - 10$, $10.1 - 15$, $15.1 - 20$, and $20.1 - 25$) were established. These wind categories are similar to those used in section 6.5 of the Crawford and Hudson report (1970).

The table reflects the basic characteristics of the three parameters: wind direction is usually northerly or southerly, wind speed increases with height, and the stability tends toward the weakly stable category with increasing height. More specifically, in the unstable condition highest probabilities occur with 5 to 10 m sec^{-1} north winds at 400 m, whereas at 23 m there is a nearly even distribution between north and south winds. High probabilities of north winds at 400 m in the unstable condition was found to be typical following strong cold fronts, regardless of the time of day. The preferred direction is south for all other classes of thermal stratification. Near the top of the tower, the tendency is toward lighter winds with decreasing stability. The converse is true at 23 m.

Stability was also calculated as a function of speed shear (wind speed at the top of the layer minus the wind speed at the bottom). Table 5 shows that the speed shear increases as stability increases at 23 m. In fact, strongly stable cases at 23 m were associated with shear speeds in excess of 8 m sec^{-1} , while unstable cases had the highest probabilities with speed shears of 0 to 1.9 m sec^{-1} . Under unstable conditions momentum is transported downward, whereas in stable cases this is not the case. In the latter instance, downward momentum transport is suppressed by atmospheric stability and light winds, but strong shears prevail near the surface. Approaching the top of the tower, the shear tends to decrease in stable stratification. In unstable cases, the shear remains low in mid- and upper levels as it does near the surface.

4.4 Persistence

Lapse rate was analyzed for persistence, defined here as the number of consecutive observations (hours) in which the lapse rate remained in the same category (table 6). The same four lapse rate categories of SS, MS, WS, and U (given in table 6) were used. For example, given an observation at 23 m in which the lapse rate first became strongly stable, the lapse rate persisted in this category for more than 12 hrs only 10 percent of the time and never persisted for more than 16 hrs.

Persistence values for a given percentage decrease with height in strongly stable and unstable cases. Strongly unstable cases had a 10 percent chance of persisting more than 10 hrs at 23 m but only 3 hrs at 400 m. Persistence values for a given percentage increase with height in weakly stable cases. The longest persistence value for WS cases was 18 hrs at 23 m and 63 hrs at 400 m.

Table 5. Thermal Stratification Versus Shear Speed (m sec^{-1}) for Three Layers (Probabilities).

| Mean Height(m) | Stability Group | <-6 | -4.1 to -6 | -2.1 to -4 | -0.1 to -2 | 0 to 1.9 | 2 to 3.9 | 4 to 5.9 | 6 to 7.9 | ≥ 8 | Sum |
|----------------|-----------------|-------|------------|------------|------------|----------|----------|----------|----------|----------|--------|
| 23 | SS | .0005 | .0004 | .0022 | .0039 | .0125 | .0207 | .0298 | .0317 | .0634 | .1651 |
| | MS | .0002 | .0010 | .0015 | .0111 | .0214 | .0369 | .0693 | .0701 | .0698 | .2813 |
| | WS | .0010 | .0039 | .0081 | .0180 | .0305 | .0477 | .0413 | .0315 | .0302 | .2122 |
| | U | .0022 | .0082 | .0216 | .0548 | .0866 | .0666 | .0556 | .0278 | .0180 | .3414 |
| | SUM | .0039 | .0135 | .0334 | .0878 | .1510 | .1719 | .1960 | .1611 | .1814 | 1.0000 |
| 133 | SS | 0 | 0 | .0012 | .0012 | .0018 | .0040 | .0059 | .0012 | .0003 | .0156 |
| | MS | 0 | .0007 | .0124 | .0342 | .0567 | .0777 | .0554 | .0084 | .0003 | .2458 |
| | WS | 0 | .0005 | .0084 | .1745 | .2567 | .1475 | .0181 | 0 | 0 | .6057 |
| | U | 0 | 0 | .0012 | .0547 | .0713 | .0057 | 0 | 0 | 0 | .1329 |
| | SUM | 0 | .0012 | .0232 | .2646 | .3865 | .2349 | .0794 | .0096 | .0006 | 1.0000 |
| 400 | SS | .0005 | .0003 | .0015 | .0030 | .0020 | .0012 | .0015 | .0007 | 0 | .0107 |
| | MS | .0007 | .0035 | .0271 | .0597 | .0843 | .0449 | .0086 | 0 | 0 | .2288 |
| | WS | 0 | .0003 | .0256 | .2811 | .3110 | .0483 | .0027 | 0 | 0 | .6690 |
| | U | 0 | 0 | .0005 | .0478 | .0417 | .0015 | 0 | 0 | 0 | .0915 |
| | SUM | .0012 | .0041 | .0547 | .3916 | .4390 | .0959 | .0128 | .0007 | 0 | 1.0000 |

Table 6. Persistence* of Lapse Rate for Six Layers and Four Stability Groups.

| Stability Group | Mean Height(m) | Persistence | | | | Maximum** |
|-----------------|----------------|-------------|-----|-----|----|-----------|
| | | 50% | 25% | 10% | 5% | |
| SS | 23 | 3 | 7 | 12 | 15 | 16 |
| | 67 | 2 | 3 | 7 | 8 | 10 |
| | 133 | 1 | 2 | 4 | 5 | 6 |
| | 221 | 1 | 2 | 2 | 3 | 5 |
| | 310 | 1 | 2 | 3 | 3 | 3 |
| | 400 | 1 | 2 | 3 | 3 | 3 |
| MS | 23 | 2 | 5 | 9 | 12 | 16 |
| | 67 | 3 | 6 | 9 | 11 | 15 |
| | 133 | 3 | 6 | 10 | 12 | 16 |
| | 221 | 2 | 5 | 8 | 11 | 17 |
| | 310 | 2 | 4 | 7 | 10 | 18 |
| | 400 | 2 | 4 | 7 | 8 | 24 |
| WS | 23 | 1 | 3 | 6 | 9 | 18 |
| | 67 | 2 | 4 | 8 | 11 | 22 |
| | 133 | 3 | 6 | 12 | 18 | 41 |
| | 221 | 2 | 6 | 12 | 18 | 39 |
| | 310 | 3 | 8 | 16 | 21 | 45 |
| | 400 | 4 | 7 | 13 | 19 | 63 |
| U | 23 | 6 | 8 | 10 | 11 | 14 |
| | 67 | 3 | 6 | 8 | 9 | 13 |
| | 133 | 1 | 2 | 4 | 5 | 7 |
| | 221 | 2 | 3 | 4 | 5 | 10 |
| | 310 | 1 | 2 | 3 | 4 | 7 |
| | 400 | 1 | 2 | 3 | 4 | 6 |

* Percent of the time that the lapse rate remained in a stability class for the indicated number of hours.

** The column indicating "Maximum" gives the maximum number of hours of persistence for any given layer and stability category.

The diurnal effect is dominant in this analysis because of radiative heating and cooling near the surface; however, diurnal effects are less pronounced near the top of the tower. Continuous moderately stable conditions exceeded 20 hrs only at 400 m and only on two occasions. All other cases exceeding 20 hrs were weakly stable.

5. INVERSION CHARACTERISTICS FOR DIFFERENT VARIABLES

5.1 Frequency of Inversions by Hour and Layer

We here discuss conditions of the thermal inversions, i.e., $\delta \leq 0$, with respect to time, air mass and cloud cover. Effects of wind speed and direction were given in the previous section.

Table 7a presents the frequency of inversions by hour and layer. There are important differences between the frequency of inversions at the bottom of the tower and near the top. Near the surface, inversions form quickly after sunset because of heat losses by longwave radiation and are most frequent just prior to midnight; thereafter, there is a gradual downward trend in frequency. (This agrees with the results of Flower, 1937.) Higher in the tower layer, inversions form more slowly after sunset, and the time of maximum frequency occurs later at the higher levels. Throughout the night there is a general increase in the frequency in the top three layers. The maximum frequency at 400 m is at 0800, well after the mean sample sunrise time. At 221 and 310 m the maximum is at 0700. At the top of the tower layer, inversions persist long after sunrise. The 34 inversions reported at 1200 in the topmost layer represent nearly 20 percent of the total observations. The reason for the post-sunrise maxima and the persistence of inversions after sunrise is due to strong low level, dissipating inversions being lifted by convective processes to heights several hundred meters above the ground. This is discussed in more detail in section 6.3.

Table 7b shows inversions of magnitude less than or equal to $-4^{\circ}\text{C}/100\text{ m}$ (strong inversions) for each layer. The obvious difference from table 7a is a general decrease in the number of observed strong inversions. The decrease is so substantial above 100 m that, prior to sunrise, strong inversions represent at most only 4 percent of the total observations. There are few changes of the maximum frequency with respect to time except in layer 3 (133 m). Here the peak shifts from 0300 to 0800 indicating that strong inversions at this level are also caused by the lifting of strong surface inversions by convective processes after sunrise instead of by radiational cooling. This is certainly the case above 200 m.

We may conclude that strong inversions formed by radiational cooling are confined mainly to layers below 100 m, and that inversions above 100 m are rarely caused directly by longwave radiation but rather by the lifting of inversions after

Table 7. Frequency of Inversion By Hour and Layer

(a) $\delta \leq 0^\circ\text{C } 100 \text{ m}^{-1}$

(b) $\delta \leq -4^\circ\text{C } 100 \text{ m}^{-1}$

| LST | Mean Height (m) | | | | | | Hour | Mean Height (m) | | | | | |
|-----|-----------------|----|-----|-----|-----|-----|------|-----------------|----|-----|-----|-----|-----|
| | 23 | 67 | 133 | 221 | 310 | 400 | | 23 | 67 | 133 | 221 | 310 | 400 |
| 0 | 128 | 85 | 74 | 63 | 59 | 47 | 0 | 50 | 12 | 3 | 0 | 0 | 1 |
| 1 | 128 | 82 | 78 | 73 | 58 | 55 | 1 | 49 | 15 | 3 | 2 | 0 | 1 |
| 2 | 125 | 89 | 85 | 69 | 64 | 52 | 2 | 47 | 14 | 4 | 2 | 1 | 1 |
| 3 | 123 | 92 | 90 | 68 | 59 | 59 | 3 | 45 | 16 | 2 | 3 | 1 | 3 |
| 4 | 127 | 91 | 81 | 77 | 69 | 57 | 4 | 49 | 15 | 7 | 3 | 1 | 2 |
| 5 | 123 | 88 | 83 | 79 | 72 | 64 | 5 | 41 | 15 | 7 | 5 | 3 | 3 |
| 6 | 117 | 86 | 87 | 80 | 75 | 75 | 6 | 46 | 17 | 6 | 3 | 4 | 3 |
| 7 | 94 | 68 | 81 | 87 | 83 | 77 | 7 | 33 | 16 | 10 | 3 | 3 | 3 |
| 8 | 58 | 52 | 65 | 78 | 73 | 79 | 8 | 20 | 9 | 11 | 5 | 3 | 5 |
| 9 | 10 | 19 | 36 | 55 | 64 | 69 | 9 | 1 | 5 | 7 | 7 | 6 | 5 |
| 10 | 0 | 4 | 22 | 33 | 41 | 55 | 10 | 0 | 0 | 3 | 5 | 4 | 4 |
| 11 | 0 | 2 | 4 | 21 | 35 | 41 | 11 | 0 | 0 | 0 | 2 | 3 | 4 |
| 12 | 1 | 2 | 3 | 9 | 19 | 34 | 12 | 0 | 0 | 0 | 1 | 0 | 4 |
| 13 | 2 | 1 | 3 | 4 | 8 | 16 | 13 | 0 | 0 | 0 | 0 | 0 | 1 |
| 14 | 4 | 3 | 3 | 3 | 6 | 14 | 14 | 0 | 0 | 0 | 0 | 0 | 0 |
| 15 | 1 | 2 | 1 | 2 | 3 | 10 | 15 | 0 | 0 | 0 | 0 | 0 | 1 |
| 16 | 0 | 0 | 2 | 3 | 1 | 8 | 16 | 0 | 0 | 0 | 0 | 0 | 1 |
| 17 | 41 | 2 | 4 | 4 | 5 | 11 | 17 | 2 | 0 | 0 | 0 | 0 | 0 |
| 18 | 106 | 16 | 10 | 4 | 6 | 15 | 18 | 21 | 0 | 0 | 0 | 0 | 0 |
| 19 | 130 | 52 | 20 | 10 | 15 | 18 | 19 | 52 | 1 | 0 | 0 | 0 | 0 |
| 20 | 131 | 82 | 47 | 26 | 25 | 25 | 20 | 54 | 1 | 0 | 0 | 0 | 0 |
| 21 | 126 | 87 | 57 | 32 | 32 | 33 | 21 | 53 | 4 | 0 | 0 | 0 | 0 |
| 22 | 130 | 83 | 68 | 50 | 49 | 37 | 22 | 60 | 7 | 0 | 0 | 0 | 0 |
| 23 | 134 | 83 | 62 | 59 | 50 | 42 | 23 | 52 | 8 | 0 | 1 | 0 | 1 |

Maximum = 174

sunrise and other factors such as thermal advection, subsidence or radiational cooling from low-level clouds and ground-based fog. The last three criteria are treated in the next section.

5.2 Frequency of Inversions by Air Mass and Layer

5.2.1 Air Mass Criteria for Oklahoma

Air mass types were determined with the aid of the Daily Weather Map Series (U.S. Department of Commerce, 1966-7). Three principle air masses are frequent in Oklahoma: continental polar (cP), maritime tropical (mT), and continental tropical (cT). The first two are more common than the latter, which occurs mainly in the early spring.

Continental polar air masses occur mostly in the winter or early spring but in this sample were also fairly frequent in the late spring. Maritime tropical air masses were observed rarely in December 1966 but showed increasing frequency from January to May 1967.

These three air masses were subdivided according to the important features in each. Table 8 gives the air mass with subscripts denoting the important features. The subscript "o" would appear to be a catchall subgroup for cases not fitting the other specific categories. Rather, this category usually fits the regular transition of air mass patterns and was characteristically one of weak gradients. It was most often associated with the break-down of stagnant high pressure cells at the surface and weak zonal flow aloft.

Table 8. Air Mass Subgroups

| Air Mass | Suffix Designation |
|---------------|-----------------------------------------------|
| cPw, cTw | Highest pressure west of station |
| cPe, cTe | Highest pressure east of station |
| cPn | Highest pressure north of station |
| cPs, cTs | Highest pressure south of station |
| cPex | Extratropical depression NE of station |
| cPt, cTt, mTt | Lee trough west of station |
| cPovr | Over-running-inverted trough south of station |
| cPsf, mTsf | Semi-stationary front north of station |
| cPo, cTo, mTo | No dominant feature |

5.2.2 Application of Air Mass Criteria to Inversion Conditions

Certain types of inversions appear to be favored in different air masses and air mass subgroups. Table 9 shows the relative frequency of inversions for the eleven most common air mass subgroups. Six subgroups have been omitted because their sample size was too small. Frequencies in table 9 are relative to the total number of observations, about half of which occur during daylight hours when inversions are rare in lower levels. Thus, low-level relative frequencies should indicate a higher probability of inversions than shown (i.e., assume inversions are primarily a nocturnal phenomenon).

All subgroups have a maximum in the 23 m layer, except the over-running situations for cP air masses. A maximum in this layer indicates that surface radiational cooling is the dominant factor; other factors such as advection⁹ and subsidence are responsible for inducing inversions primarily at upper levels, as conditions of the free atmosphere are approached (Staley and Jurica, 1968). Radiational cooling from cloud tops is another factor at upper tower levels in certain meteorological situations.

The cPs air mass subgroup tends to form low-level nocturnal inversions most often (63.9 percent at 23 m). In other cP subgroups the tendency for low-level inversions is somewhat lower. The cPovr air mass subgroup has a distinct minimum in the lower levels. It is radically different from other subgroups in all respects. Over-running situations are often characterized by low stratus clouds or fog inhibiting surface inversions. If low-level radiational cooling was the only cause of inversions in the tower layer, then the frequency of inversions would be expected to decrease with height. If other causes of inversions, having effects only at upper levels were present, then a systematic decrease in the frequency of inversions would not be expected or would, at least, be small.

Inversion potential in five of the eleven subgroups (cPs, cPe, cPo, mT_φ, cTt) decreases with height. Except for the cPe subgroup, we may conclude that long-wave radiation accounts for most of the inversions in the remaining four subgroups. In the cPe subgroup, the decrease is quite slow and the definition of the subgroup implies that factors such as warm advection or subsidence may be important. Subsidence is probably responsible for the secondary peak at 400 m in the cPn subgroup

⁹ Advection referred to here (specifically warm advection) is that which is present on the "back" or west side of cP highs. This sometimes appears in the Southern Great Plains as a weak warm front or temperature/moisture discontinuity whose forward slope insures that the warm advection be most pronounced aloft first. Cold advection is also a source of inversions in the boundary layer. These types of inversions are observed in the surface outflow of thunderstorms. They determine the discontinuity between the shallow cold air outflow of the thunderstorm and the warmer inflow air above. They constitute a small percentage of inversions in mT air masses.

Table 9. Relative* Frequency (percent) of Inversions by Air Mass and Layer.

| Air Mass Subgroup | Mean Height (m) | | | | | |
|-------------------|-----------------|------|------|------|------|------|
| | 23 | 67 | 133 | 221 | 310 | 400 |
| cPw | 56.0 | 39.1 | 32.3 | 22.7 | 13.5 | 17.8 |
| cPe | 58.1 | 46.4 | 47.9 | 41.8 | 35.0 | 32.4 |
| cPn | 43.6 | 26.3 | 16.3 | 14.1 | 18.2 | 24.2 |
| cPs | 63.9 | 52.6 | 52.6 | 40.2 | 24.8 | 21.8 |
| cPt | 57.2 | 33.3 | 48.3 | 51.1 | 44.4 | 31.1 |
| cPovr | 4.5 | 3.8 | 6.0 | 10.3 | 16.3 | 25.0 |
| cPo | 60.0 | 50.8 | 44.4 | 31.8 | 29.8 | 24.1 |
| mTt | 36.9 | 9.9 | 12.1 | 20.8 | 26.7 | 25.6 |
| mTsf | 48.7 | 27.9 | 31.4 | 27.4 | 22.8 | 19.7 |
| mTo | 46.9 | 34.0 | 36.0 | 33.5 | 29.3 | 21.6 |
| cTt | 49.1 | 36.4 | 31.7 | 30.0 | 14.4 | 13.2 |

* Relative to the total number of observations for each subgroup.

and warm advection is important at high levels in cPt, cPovr and mTt air mass subgroups (secondary or primary peaks above 200 m). The secondary maximum at high levels in mTt air masses is very pronounced with a distinct minimum at 67 m. That this air mass subgroup is so stable at night is interesting in view of speculations by Kessler and Bumgarner (1971) about stable boundary layer conditions believed necessary for nocturnal thunderstorms. Nocturnal thunderstorms are frequently observed in this air mass subgroup. Cloud top radiation is an additional factor in the cPovr category. Little can be inferred from the meteorological situation about the behavior of the mTsf subgroup. It has characteristics similar to the mTo subgroup.

5.3 Frequency of Inversions by Cloud Cover and Layer

5.3.1 Cloud Cover Characteristics for Oklahoma

The most important factors influencing the lapse rate characteristics in certain parts of the tower layer are the height, extent and depth of cloud cover. Hourly observations of cloud cover were obtained from Oklahoma City Weather Bureau records and codified in detail according to height and extent. The thickness of cover was not available. It was found that similar lapse rate characteristics occurred in the following broad cloud cover groups:

- (a) Clear skies,
- (b) Cirrus clouds only - scattered, broken or overcast,
- (c) Partly cloudy skies - broken or scattered middle and/or low clouds (including cirrus when lower clouds were observed),
- (d) Overcast - middle or low clouds including fog.

5.3.2 Application of Cloud Cover Criteria to Inversion Conditions

Table 10a shows the frequency of inversions by cloud cover group and layer, and table 11a is the corresponding relative frequency. The total observations for each cloud group are given on the right in table 10a. With clear observations, there is a systematic decrease with height in the number of inversions. With a cirrus cloud cover, the relative frequency of inversions near the surface is substantially reduced, but a cirrus cover does not reduce the relative frequency of inversions near the top of the tower compared to the relative frequency in clear skies. With partly cloudy and overcast conditions the effect at the lower levels is more pronounced, but there is still only a small influence of cloud cover on high level inversions. It was pointed out in the previous section that high-level boundary layer inversions are influenced more by factors such as the air mass (subsidence or advection) or the time of day (the lifting of a low-level inversion after sunrise), rather than radiation. Since low-level inversions are caused primarily by radiational cooling,

Table 10. Frequency of Inversions by Cloud Cover Group and Layer

| Cloud Cover Group | (a) $\delta \leq 0^\circ\text{C } 100 \text{ m}^{-1}$ | | | | | | Total Obs. |
|-------------------|-------------------------------------------------------|-----|-----|-----|-----|-----|------------|
| | 23 | 67 | 133 | 221 | 310 | 400 | |
| Clear | 925 | 675 | 585 | 501 | 410 | 364 | 1405 |
| Cirrus only | 562 | 341 | 302 | 271 | 269 | 266 | 1095 |
| Partly cloudy | 272 | 115 | 119 | 131 | 167 | 183 | 823 |
| Overcast | 66 | 32 | 52 | 21 | 121 | 174 | 835 |

| Cloud Cover Group | (b) $\delta \leq -4^\circ\text{C } 100 \text{ m}^{-1}$ | | | | | | Total Obs. |
|-------------------|--------------------------------------------------------|-----|-----|-----|-----|-----|------------|
| | 23 | 67 | 133 | 221 | 310 | 400 | |
| Clear | 425 | 107 | 36 | 21 | 7 | 13 | 1405 |
| Cirrus only | 207 | 37 | 19 | 18 | 14 | 9 | 1095 |
| Partly cloudy | 34 | 6 | 7 | 2 | 5 | 12 | 823 |
| Overcast | 1 | 1 | 0 | 1 | 3 | 8 | 835 |

cloud cover of any type and height absorbs longwave radiation emitted from the earth and reradiates part of this energy back to earth, thus, preventing the formation of low-level inversions. Notice that the behavior of the relative frequency of inversions with height for overcast skies is similar to the behavior of the corresponding relative frequency for cPovr air masses (table 9). The two are often synonymous but the former is more general.

Tables 10b and 11b give the frequencies and relative frequencies of inversions less than or equal to lapse rates of $-4^{\circ}\text{C } 100 \text{ m}^{-1}$, respectively. The same general characteristics from earlier tables (10a and 11a) are applicable here, except that frequencies and relative frequencies are much reduced. Above 200 m these strong inversions occur less than 2 percent of the time and are quite rare at any height under overcast skies.

6. CASE STUDIES

6.1 A Sequence of Changing Air Masses Associated With an Extra-tropical Cyclone

Three distinct air masses are often associated with the passage of an extra-tropical cyclone during the late winter and spring months in the Southern Great Plains: maritime tropical (mT), continental tropical (cT) (see footnote 8, page 17), and continental polar (cP). They affect a given location in the order indicated. In the spring when specific

Table 11. Relative Frequency (percent) of Inversions by Cloud Cover Group and Layer

| Cloud Cover Group | (a) $\delta \leq 0^{\circ}\text{C } 100 \text{ m}^{-1}$ | | | | | |
|-------------------|---------------------------------------------------------|------|------|------|------|------|
| | 23 | 67 | 133 | 221 | 310 | 400 |
| Clear | 65.8 | 43.0 | 41.6 | 35.7 | 29.2 | 25.9 |
| Cirrus only | 51.3 | 31.1 | 27.8 | 24.8 | 24.6 | 24.3 |
| Partly cloudy | 33.0 | 14.0 | 14.5 | 15.9 | 20.3 | 22.2 |
| Overcast | 7.9 | 3.8 | 6.2 | 9.7 | 14.5 | 20.8 |

| Cloud Cover Group | (b) $\delta \leq -4^{\circ}\text{C } 100 \text{ m}^{-1}$ | | | | | |
|-------------------|----------------------------------------------------------|-----|-----|-----|-----|-----|
| | 23 | 67 | 133 | 221 | 310 | 400 |
| Clear | 30.2 | 7.6 | 2.6 | 1.5 | 0.5 | 0.9 |
| Cirrus only | 18.9 | 3.4 | 1.7 | 1.6 | 1.3 | 0.8 |
| Partly cloudy | 4.1 | 0.7 | 0.9 | 0.2 | 0.6 | 1.5 |
| Overcast | 0.1 | 0.1 | 0.0 | 0.1 | 0.4 | 1.0 |

humidities in the maritime air mass are high and the upper atmosphere is sufficiently cool, severe storms often occur along and ahead of the boundary separating the mT and cT air masses. In this report, the two boundaries separating the three air masses associated with an extra-tropical cyclone will be called a double front.

Two such double front events occurred during the three day period 21-23 April 1967. A time section of temperature, winds, moisture and cloud cover was plotted (fig. 9) using 5-min means centered at the start of the hour. Moisture and cloud cover was plotted (fig. 9) using 5-min means centered at the start of the hour. Moisture (dew points and relative humidity) and cloud information were taken from the Oklahoma City Weather Bureau records. The cloud data are in three digit code form. The first digit refers to low clouds (≤ 5000 ft), the second refers to middle clouds (> 5000 ft but less than 15,000 ft) and the last refers to high clouds ($\leq 15,000$ ft). Each of the three digits range in value from 0 to 3 as follows:

| | |
|---|--------------------|
| 0 | no clouds |
| 1 | scattered clouds |
| 2 | broken cloud cover |
| 3 | overcast skies |

Maritime tropical air is assumed to be present in the whole tower layer at the beginning of the period. This cannot be confirmed because humidity values are not available from the top of the tower but the wind direction profile is fairly uniform and south winds dominate. The wind conditions have persisted for more than 12 hrs before the initial time. Between 0300 and 0500 on 21 April the winds begin to veer above 400 m which coincides with some cloud dissipation. At 0800, high level veering is quite pronounced, producing strong directional shears in the tower layer. It is assumed that this veering is a manifestation of the arrival of cT air at the higher levels. The slope of the "front"¹⁰ is assumed to be small.

Since this event occurred so early in the morning, there was little surface heating, and convective activity did not develop. The passage of the cT "front" is difficult to detect in the wind speed and temperature fields; however, a rapid decrease in the dew point is evident and typifies these "fronts." The slope of the "front" cannot be computed, since the horizontal speed is unknown, but the wind direction at 444 m begins to veer at 0400 and at the surface 6 hrs later. For a speed as small as 5 m sec^{-1} , the slope estimated from the wind shift times is roughly 1 to 230. The gradual wind shift and small slope of

¹⁰The definition of the term "front" is rather loose in this section and is not used as in the strict Norwegian school. The term "front" as applied to cT air mass incursions into central Oklahoma is used in the same sense as dry lines along which deep convection has developed. In the latter case the slope is quasi-vertical (McGuire, 1962).

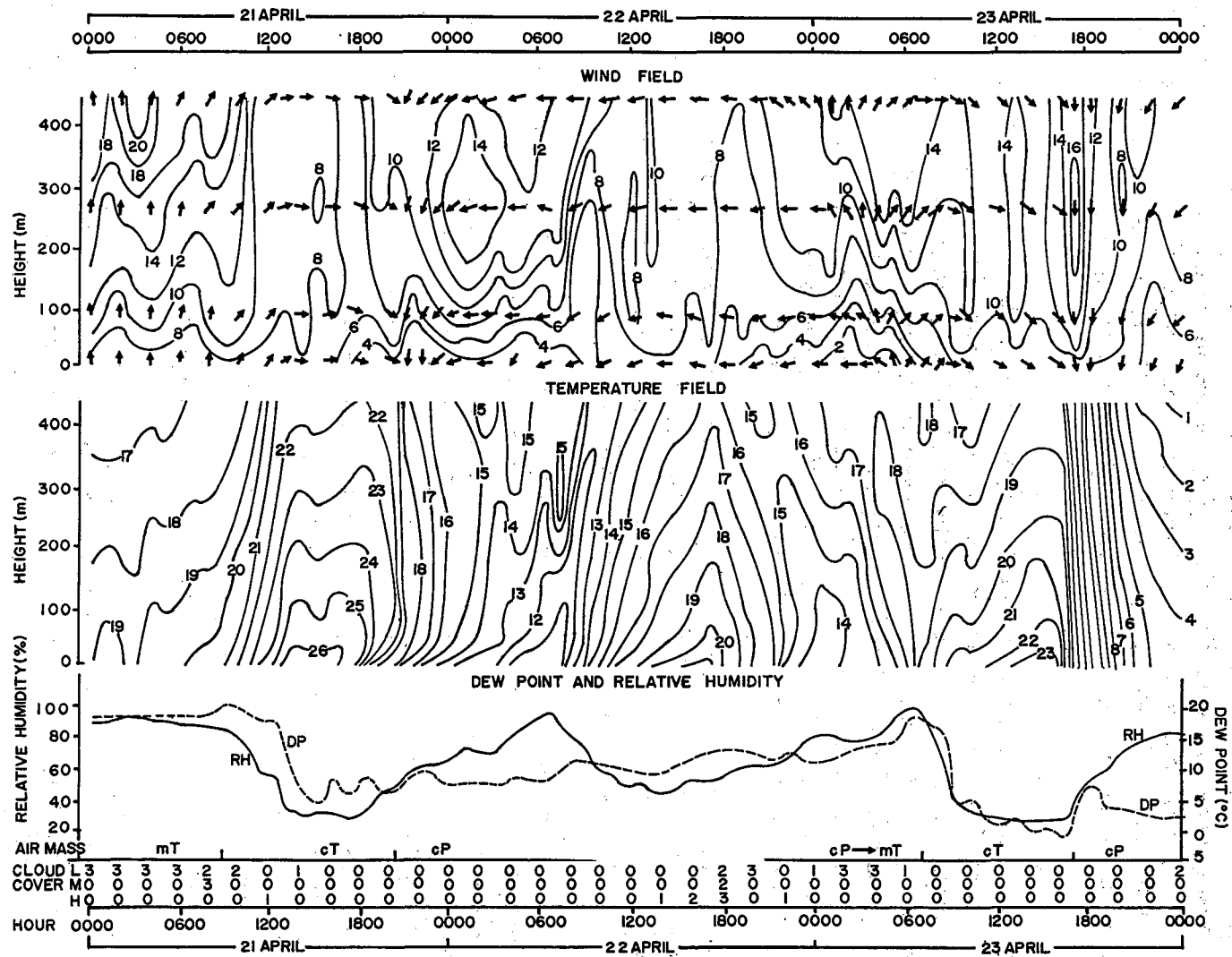


Figure 9. A sequence of changing air masses (21-23 April 1967). Isotachs in m sec^{-1} , isotherms in $^{\circ}\text{C}$.

the cT "front" are not typical of the dry line common in the Southern Great Plains, although both are similar in other respects. The cT air does not remain long. In the two double front cases, cT air is present between 8 and 10 hours.

The change from cT to cP air at about 2000 on 21 April occurs with a sharp discontinuity in the temperature and wind direction. The change in the dew point is insignificant, and the rise in the relative humidity is of diurnal nature. The wind speed is relatively unchanged in this record. Since both air masses are relatively dry, there is no convective activity. This is typical of continental polar fronts when they replace continental tropical air.

The return of mT air early on 23 April is even more subtle than the cT frontal passage. There are similarities between the two in that the slope of the weak warm front (mT) is quite small. In addition, there are similar directional shears in the tower layer as the slightly sloping "front" passes through the tower layer (moisture changes, however, mark these two fronts). The wind at 444 m begins to veer 8 hrs before veering at the surface. At 0300, 23 April, there is about 120° of vertical direction veering from the surface to 444 m. In this case, the substantial direction shear maybe caused by the strong inversion present. For a 5 m sec^{-1} forward speed, the slope is estimated to be 1 to 310.

The dew point increases very gradually during the transition from polar to maritime air. The relative humidity shows large diurnal fluctuations and is less reliable as a frontal indicator. During the transition, there is a short period of low overcast conditions, as the warm moist air overrides the colder air near the surface.

Continental tropical air returns around 0900 on 23 April. The dew point drops very rapidly (as does the relative humidity), and the wind shifts to the west or northwest at all levels. Continental tropical frontal passages can be distinguished from cP frontal passages by the lack of subsequent cold advection. The maximum temperature on 23 April is 2°C warmer than the previous day when cP air was present.

The last event in the three day sequence is a very strong cP cold front at 1700 on 23 April. The cold advection is pronounced but is enhanced by diurnal cooling. The wind is from the north and northeast and is quite strong at the frontal discontinuity. Although the dew point remains low, there is some increase in the vicinity of the front.

6.2 A Warm Frontal Passage

Classical warm fronts are frequently associated with extra-tropical cyclones in Oklahoma in the winter months. An example of such a warm front occurred on the night of 31 January and 1 February 1967. The event was complicated by the presence of a strong surface inversion before the frontal passage which blocked the downwind propagation of warm air.

Profiles determined during the course of the night are illustrated in figure 10. The pre-front boundary layer conditions are represented by profile #1 at 1957, 31 January. A strong surface inversion about 100 m deep is evident and nearly isothermal conditions exist above the inversion. During the 20 min following 1957, there is cooling near the surface and gradual warming above 100 m. In the upper layer, there is some indication of more heating above 400 m than below. This is clearly the case at 2147 (profile #3). At 2212, the heating presumably caused by warm advection has progressed down to 300 m. Thus, in 55 min the warm front, indicated by the upper level discontinuity, has only propagated downward 100 m. The northward speed of the front at the surface was determined from weather maps to be 8 to 10 m sec⁻¹. The slope of the front is, therefore, roughly 1 to 360.

The profile at 2302 indicates that the frontal discontinuity has reached 150 m above the surface. The depth of the surface inversion during the time period between the first and fifth profile (3 hrs, 5 min) has grown to 150 m. When the frontal discontinuity reaches the top of the very stable surface layer, the warm air has difficulty dislodging the dense colder air. Two hours elapse between profiles 5 and 6 during which the warm air has penetrated only another 50 m. This is shown schematically in figure 11. In the diagram, the abscissa is compressed considerably with respect to the ordinate.

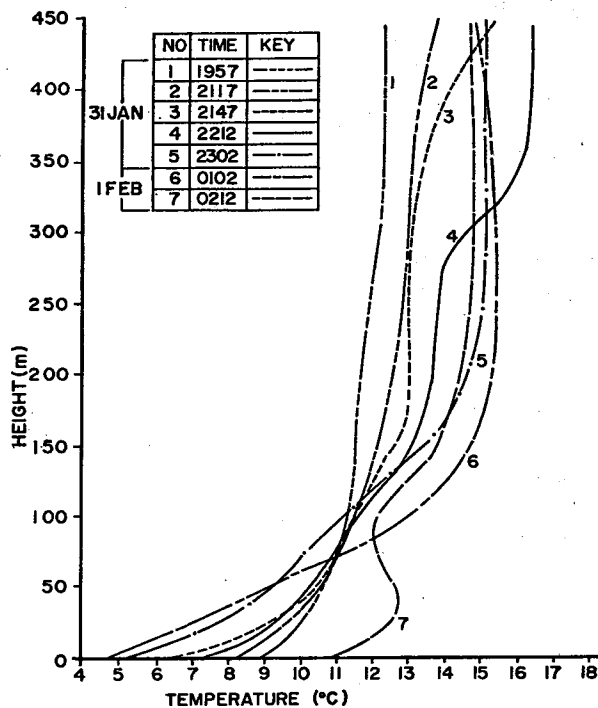


Figure 10. Selected temperature profiles during the 31 January - 1 February '67 warm frontal passage.

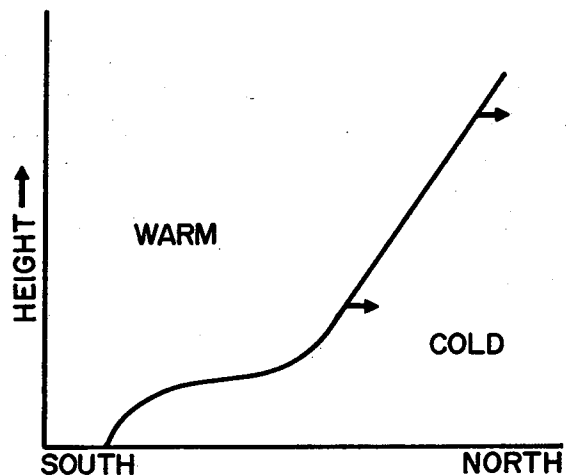


Figure 11. Schematic diagram of the 31 January - February '67 warm front.

If figure 11 adequately represents the time to space conversion, we may conclude that the forward speed of the warm front is somewhat greater above the inversion than at the surface. Thus, the slope of the front above the inversion is correspondingly smaller than indicated earlier. The warm front reaches the surface between profiles 6 and 7 when the 2 m temperature increases more than 6°C in 70 min.

6.3 A Dissipating Inversion After Sunrise

The mean lapse rate characteristics are discussed in earlier sections. In data adjusted for variations in the sunrise time, nocturnal inversions, especially in clear and dry air masses, are commonplace in the tower layer and persist long after sunrise. The strongest inversions occur in the winter months.

A mid-winter low-level inversion (12 February 1967) was chosen from the 6 month sample and analyzed in detail by determining 5 min mean temperatures from the strip charts and calculating the lapse rate per 100 m from these temperatures. Figures 12 and 13 show the predawn inversion and its dissipation during the transition period. The dashed line in figure 12 is a curve indicating a minimum temperature. At most levels, this was the lowest temperature for the previous 18 hrs. This was a secondary minimum for the same period at 444 m. The dashed line in figure 13 is also a minimum temperature curve. The letters "P" and "S" denote primary and secondary minima, respectively, for the specified 18 hr period. The dotted line denotes the strongest portion of the inversion. The minimum temperature curve lags the inversion maximum curve by several tens of minutes. That the daily minimum temperature occurs after sunrise some distance above the surface is generally known (see section 3), but the mechanism responsible is not well defined. A possible mechanism will be described.

The predawn inversion is about 250 m deep and is strongest between 50 and 100 m. Apparent lifting of the inversion base begins immediately after sunrise. At this time, a condition depicted in figure 14 (T) is occurring where the bottom of the inversion is being heated and there are only insignificant height changes occurring at mid and upper levels. This is shown by the arrows labeled A and B which denote motions of the base and top of the inversion, respectively. The arrows should not be construed as vectors as they only show direction. Notice that the top of the inversion is actually lower (0° isopleth, fig. 13) at 0802 than at sunrise. This condition of heating at the base of the inversion with little or no lifting of the whole inversion will be called the "preconvection stage" of the breaking inversion.

At about 0900, the slope of the inversion maximum curve begins to steepen, indicating the onset of the second stage of the breaking inversion. This will be called the "convection-induced-lifting stage." The inversion now begins to dissipate quite rapidly.

A neutrally stratified convective layer separates a low-level superadiabatic layer from the inversion. The convective layer is filled with plumes and thermals (Warner and

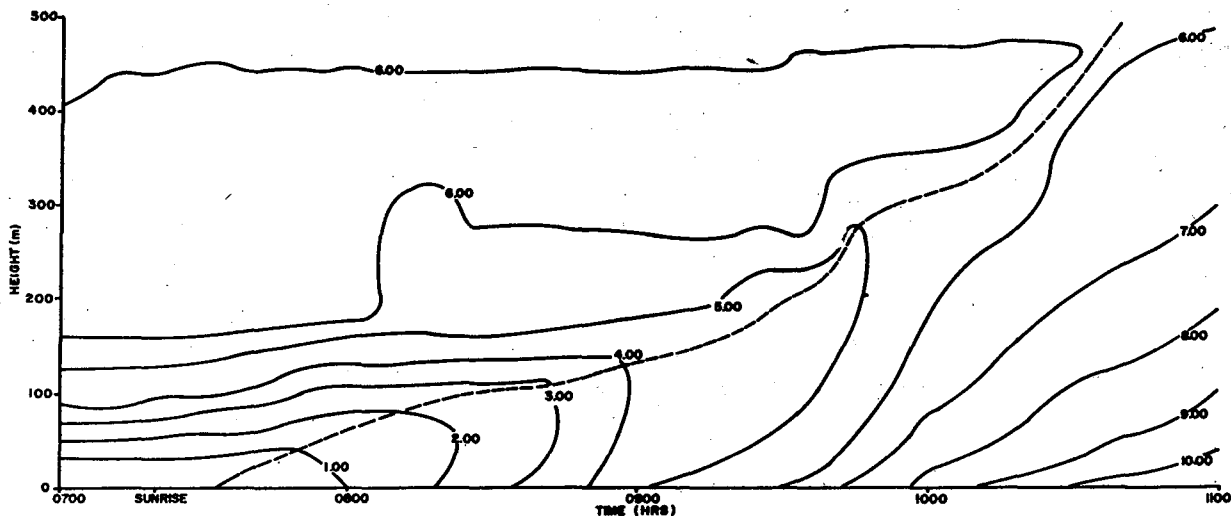


Figure 12. Temperature time section during a dissipating morning inversion. 12 February 1967. Temperatures in °C.

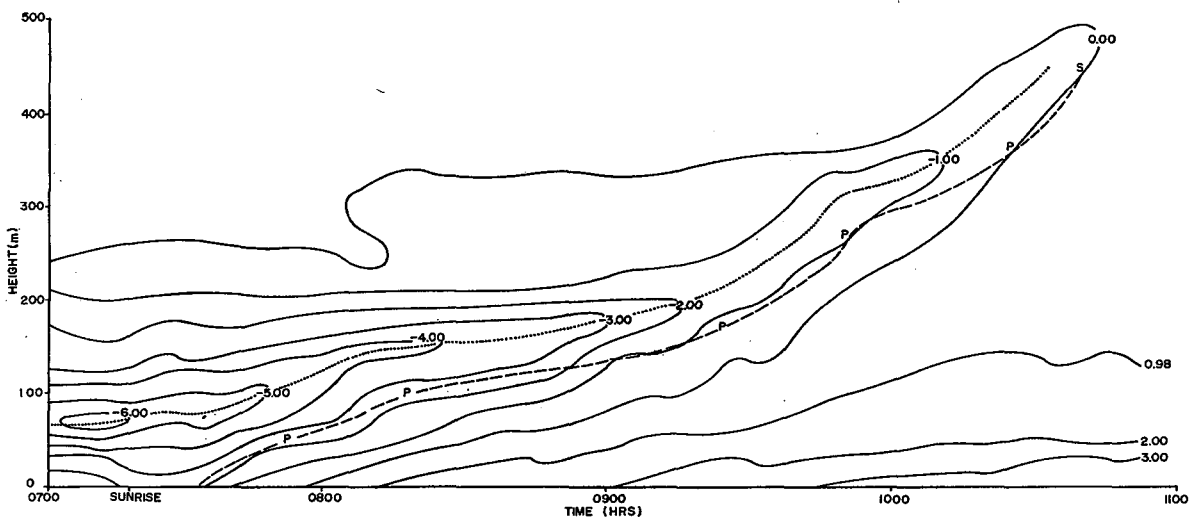


Figure 13. Lapse rate ($^{\circ}\text{C } 100 \text{ m}^{-1}$) time section during a dissipating morning inversion. 12 February 1967.

Telford, 1967). These elements lift masses of warm air to the base of the inversion. The buoyancy of the parcels initially warmer than their environment overshoot (convective overshoot) the base of the inversion (Plate, 1971; Ball, 1960). After penetrating the inversion a short distance they enter a region where they are cooler than their environment and sink. The entrainment of a thin layer at the base of the inversion occurs when energy cascades from the larger scale of the convective elements to turbulent scales. Plate indicates that the inversion is dissipated only by entrainment of the stable air into the convective layer. This conclusion was drawn from the diagrams of Warner and Telford (1967); these show no apparent change in the temperature above the top of the inversion, implying that the whole inversion is not being physically lifted, which is contrary to observation of the 12 February, Oklahoma City inversion, those of Fanaki (1970) in a laboratory model, and Ball (1960). Ball points out that subsidence retards upward motion of the inversion which may be the case in Warner and Telford's observation. Ball's estimate of the height change of the inversion (150 m hr^{-1}) is consistent with that derived from figure 13 between 0900 and 1000. This value is about 135 m hr^{-1} . Figure 14 (II) is a slight exaggeration of the second stage. The arrows A and B are in the direction of increasing height indicating that all portions of the inversion are being lifted.

"Convective overshoot" does not generally decrease the temperature above the entrainment layer in this case (see fig. 15); however, there is some evidence that this is occurring at 0929 (fig. 13, 275 m). Points A_1 , A_2 , A_3 and A_4 in figure 15 indicate the

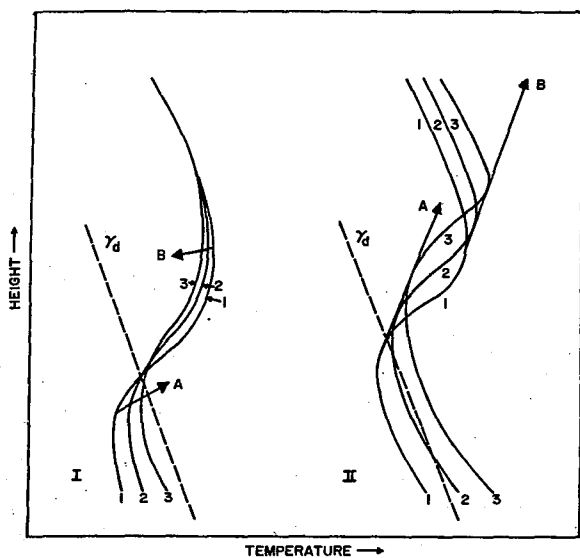


Figure 14. Preconvective and convective stages of a late morning inversion (schematic).

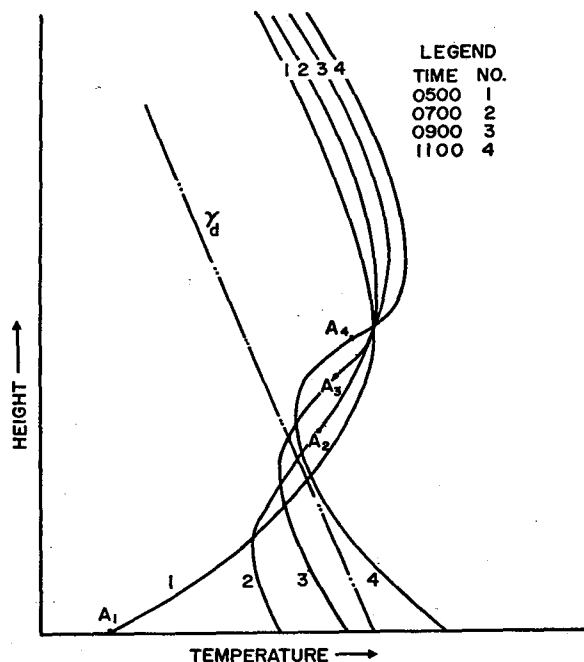


Figure 15. Profile changes during convective overshoot (schematic).

center of the intensifying inversion caused by "convective overshoot." The small decrease in the lapse rate is not conclusive because it does not exceed instrument tolerances. It was mentioned in the beginning of this section that diurnal minimum temperatures are often observed after sunrise. More specifically, minimum temperatures occur at the time when the base of the inversion is lifted past a given level. "Convective overshoot" tends to cool the inversion base and, thus, increases the probability that the diurnal minimum temperature occurs at this time.

The growth of the convective layer may be predicted by integrating the conservation of heat equation (Deardorff, et al., 1969) or by simplifying the turbulent-energy equation (Ball, 1960).

$$h^2 = \frac{2(H_h - H_o)t}{\rho c_p \gamma_s} \quad (1)$$

where h is the depth of the convective layer, H is the heat flux (subscripts h and o referring to heights of the base of the inversion and the top of the autoconvective layer), t is time, ρ is density, c_p is the specific heat at constant pressure and γ_s is the mean lapse rate in the inversion. Equation (1) is useful to a first approximation (Plate, 1971). Solving for H_o , making the assumption that $H_h = -H_o$, a value of 30 watts m^{-2} is obtained. This is in close agreement with the results of Warner and Telford (1964) under similar meteorological conditions, and at the same height.

The final stage of the dissipating inversion is not shown in figures 12 or 13 because the inversion has been lifted above the tower layer. This is the adjustment stage when the temperature discontinuity disappears, and there is an adjustment in the two layers separated by the original interface. The adjustment comes in the form of heat and momentum exchange often causing large amplitude, small scale undulations in the temperature, and wind field near the top of the tower. The undulations are not shown in figures 12 or 13 because of chart smoothing. Last evidence of the morning transition period is at 1122, more than 4 hrs after sunrise.

7. SPECTRUM ANALYSIS

Spectra for the 6 mo sample were drawn for three levels on the WKY tower: 2, 90, and 444 m. Initial records contained some missing data points. These were assigned values by interpolation or, if the gap in the time series was too long, the missing points were filled in by the application of a polynomial curve determined from hourly mean temperature for the month. End points were checked for discontinuities when the latter technique was used.

Table 1 shows that a significant trend is present in the series at all three levels. The trend is steepest at 2 m. A band-pass filter (fig. 16) was designed to eliminate this trend and the "noise" at high frequencies. The filter was composed of two normal smoothing functions (see Holloway, 1958). The multiples of the sampling interval on the abscissa in figure 16 correspond to the reciprocal of the frequency values on the abscissa in figure 17 a-c.

Spectra were hanned (Blackman and Tukey, 1958) and drawn in a range of periods extending from 4.8 hrs to 37.5 days. These periods correspond to a response of 63 percent at either end of the filter. Some additional block averaging of spectra points was used to "stabilize" the spectrum at higher frequencies. There is some variance at high and low filtered frequencies due to the lack of a sharp cut-off.

Figure 17 a-c shows the spectra computed for the three levels indicated. Spectra at all three levels exhibited similar characteristics at periods typical of planetary waves (~ 10 days), and the same is true at synoptic scales (period ~ 3 days). Larger variance at planetary scales compared to synoptic scales is evident in the whole tower layer. This is different from the results of Griffith, et al. (1956) for a temperature spectrum computed from a 66 yr record near the surface in Pennsylvania. Differences between the two scales imply that in Oklahoma synoptic systems are typically weak, except when synoptic scale waves are amplified by Rossby type wave troughs. In Pennsylvania equal energy is associated with both scales.

Variance at 24 hrs at 2 m and 90 m dominates the spectrum for those two levels, but at 400 m variance is much reduced at high frequencies. There is also a fairly large peak at 12 hrs at lower levels. The decreasing variance with height at diurnal periods implies that diurnal temperature oscillations become very small as the free atmosphere is approached.

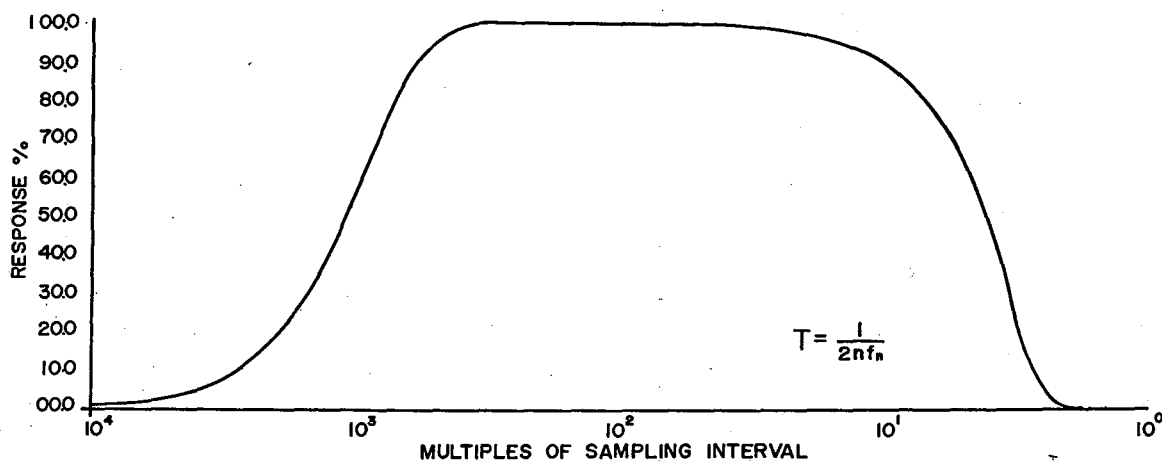


Figure 16. Band-pass filter for spectra.

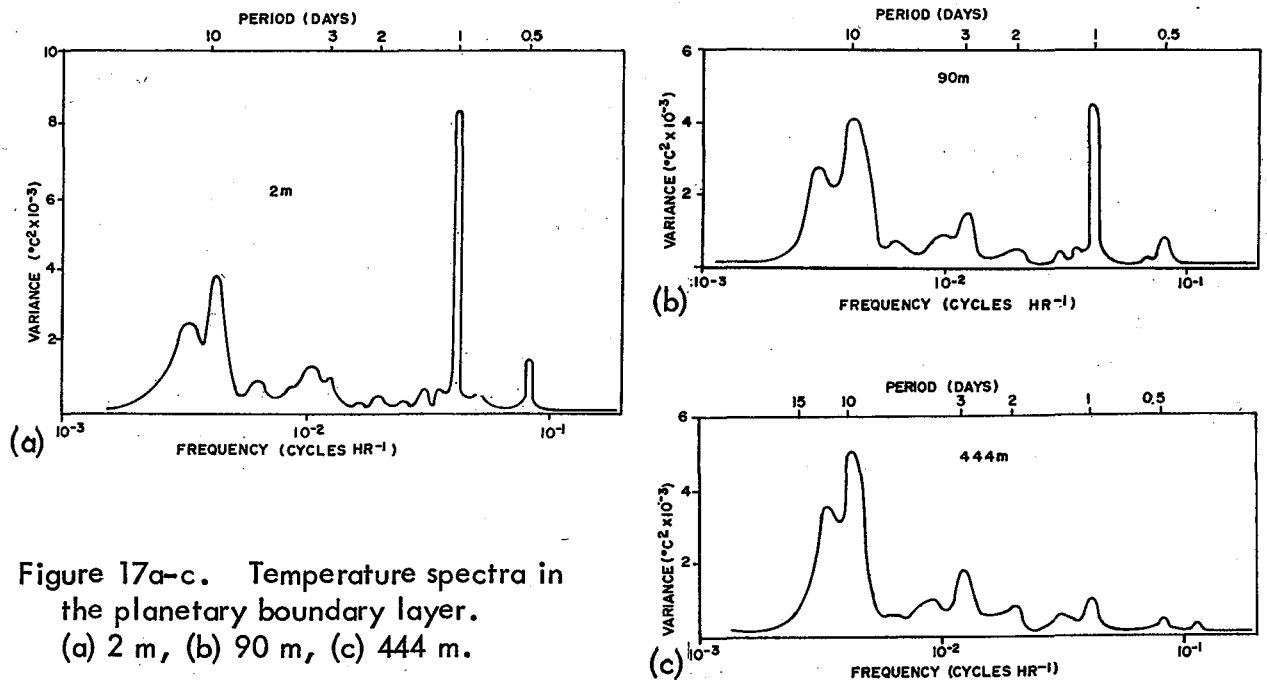


Figure 17a-c. Temperature spectra in the planetary boundary layer. (a) 2 m, (b) 90 m, (c) 444 m.

It is interesting to note that the diurnal vertical temperature pattern in nearly opposite to the wind pattern observed by Crawford and Hudson (1970). The amplitude of wind fluctuations increases with height; i.e., the amplitude of the diurnal wave at 444 m is three times that at 7 m (see fig. 11 in Crawford and Hudson, 1970). Several mechanisms are responsible for these differences. Heat conduction/longwave radiation are amplifying factors for the surface temperature and surface friction is a damping factor for the surface wind. The former causes a daily coupling and decoupling of the boundary layer with the free atmosphere, insuring a daily recurrence of downward momentum transport affecting the upper levels more than the lower levels. Little heat (or cold) is transported downward because of the thermal stratification (temperature decreases with height, typically). The source of temperature changes at 444 m most likely come from below or are advected horizontally.

8. SUMMARY AND CONCLUSIONS

A six month sample of temperature data from seven levels on the NSSL/WKY-TV tower north of Oklahoma City, Oklahoma, has been analyzed for characteristics of temperature and lapse rate.

Mean temperatures for the time series show that the sample is representative of the climatological mean. Analysis indicates that, with few exceptions, characteristics observed in Oklahoma are similar to those in England, Egypt, and Russia in comparable tower studies; however, when the data are adjusted to local sunrise and sunset, many

additional characteristics are found. An attempt was made to isolate these characteristics by grouping the data according to type of air mass or extent of cloud cover: (1) the evening transition period exhibited a tendency for high level instability at or subsequent to sunset after a late afternoon increase in stability. This occurred in clear dry air masses predominantly. (2) The morning transition lasted for many hours after sunrise. The boundary layer and the free atmosphere are often not coupled until around local noon, especially on clear dry days when the nocturnal inversion is deep and strong. (3) Maximum afternoon lapse rates at the top of the 444 m tower lag the maximum surface values by several hours. (4) Maritime tropical air masses typically have stronger inversions in mid-tower layers than near the surface at night. This may have some relationship to the well known low-level jet observed in the Great Plains in this type of general wind flow pattern.

A detailed study of inversions was made by analyzing with respect to time, air mass and cloud extent. Inversions are most common near the surface a few hours after sunset but are most frequent near the top of the tower a few hours after sunrise. Inversions in most air masses occur most frequently near the surface and the frequency generally decreases upward. The exception is the overrunning situation where a minimum occurs at the surface and the frequency increases upward. Inversions near the surface are inversely proportional to the amount of cloud cover; at 400 m, however, inversions do not appear to be a function of the cloud cover.

Of the three short case studies presented, two were concerned with frontal passages. The third was a study of a dissipating nocturnal inversion after sunrise, showing the mechanisms responsible for dissipation. The whole event was divided into three stages depending on these mechanisms. The daily minimum temperature was often observed to coincide with this dissipation, especially during the period in which the inversion is actually lifted by convective processes.

Spectra of the temperature in the range of periods from about 4 hrs to 40 days show three principle peaks at planetary, synoptic, and diurnal scales. The latter is quite pronounced at 2 m but much reduced at 444 m. This substantiates the large values of persistence (max. 63 hrs) observed at this level. There are insignificant changes in the synoptic and planetary scales with height. The planetary scale has more variance, however, indicating that every third front is a strong one; i.e., every third synoptic scale wave is amplified by a Rossby type wave.

9. ACKNOWLEDGMENTS

The authors wish to thank Dr. Edwin Kessler who suggested this study and reviewed the manuscript. The design work of the NSSL/WKY-TV meteorological tower is credited to Mr. L. D. Sanders (CEDDA, NOAA)¹¹ and Mr. John Carter. Mr. L. Johnson provided

¹¹ Formerly employed at NSSL.

technical support for the data collection. Mrs. K. Gray supervised the digitizing of the strip charts, and Mr. W. Bumgarner developed the computer programs for the spectrum analysis. Mr. W. D. Zittel is responsible for most of the statistical and graphics work. The authors appreciate the assistance and encouragement offered by Dr. S. Barnes. He and Dr. Y. Sasaki (University of Oklahoma) also reviewed the manuscript.

10. REFERENCES

- Ball, F. K. (1960), Control of inversion height by surface heating, *Quart. J. Roy. Met. Soc.*, 86, 483-494.
- Berry, F.A., E. Bollay and N. R. Beers (1945), *The Handbook of Meteorology*, McGraw-Hill Book Co., Inc., New York, 1098 pp.
- Best, A. C. (1935), Transfer of heat and momentum in the lowest layers of the atmosphere, *Geophys. Mem.*, 65.
- _____, E. Knighting, R. H. Pedlow and K. Stormonth (1952), Temperature and humidity gradients in the first 100 m of SE-England, *Geophys. Mem.*, 89.
- Blackman, R. B. and J. W. Tukey (1958), *The Measurements of Power Spectra*, Dover Publications, Inc., New York, 190 pp.
- Brocks, K. (1948), *Über den tagl. u. jahrl. Gang der Höhenabhängigkeit der temp. in den untersten 300 m d. Atmosphäre u. ihren Zusammenhang mit d. Konvektion*, *Ber. DWD-US Zone*, 1, No. 5.
- Carter, J. K. (1970), *The NSSL meteorological tower facility*, *ESSA Tech Memo.*, ERLTM-NSSL 50, 40 pp.
- Crawford, K. C. and H. R. Hudson (1970), *The behavior of winds in the lowest 1500 feet in central Oklahoma: June 1966 - May 1967*, *ESSA Tech. Memo.* ERLTM-NSSL 48, 57 pp.
- Deardorff, J. W., G. E. Willis and D. K. Lilly (1969), Laboratory investigation of non-steady penetrative convection, *J. Fluid Mech.*, 35, 7-31.
- Fanaki, F. H. (1970), A simulation of heat flux in the lower troposphere by a laboratory model, *Boundary Layer Met.*, 1, 345-367.
- Flower, W. D. (1937), An investigation into the variation of the lapse rate of temperature in the atmosphere near the ground at Ismailia, Egypt, *Geophys. Mem.*, 71.

- Geiger, R. (1965), *The Climate Near the Ground*, Harvard University Press, Cambridge, Mass., 611 pp.
- Gol'tsberg, J. A. (1967), *Microclimate of the USSR*, Israel Program for Scientific Translations Ltd., IPST Cat. No. 5345, 1969 (English translation).
- Griffith, H. L., H. A. Panofsky and I. Van der Hoven (1956), Power spectrum analysis over large ranges of frequency, *J. Meteorol.*, 13, 279-282.
- Haurwitz, B. and J. M. Austin (1944), *Climatology*, McGraw-Hill Book Co., Inc., New York, 410 pp.
- Holloway, J. L. (1958), Smoothing and filtering of time series and space fields, *Advances in Geophysics*, 4, Academic Press, New York, 351-389.
- Johnson, N. K. and G. S. P. Heywood (1938), An investigation of the lapse rate of temperature in the lowest 100 m of the atmosphere, *Geophys. Mem.*, 77.
- Kessler, E. and W. C. Bumgarner (1971), Model of precipitation and vertical air currents, NOAA Tech. Memo. ERLTM-NSSL 54, 93 pp.
- McGuire, E. L. (1962), The vertical structure of three dry lines as revealed by aircraft traverses, NSSP Report No. 7, 10 pp.
- Plate, E. J. (1971), *Aerodynamic Characteristics of Atmospheric Boundary Layers*, AEC, Div. of Tech. Inf., Washington, D. C., 190 pp.
- Saucier, W. J. (1955), *Principles of Meteorological Analysis*, The University of Chicago Press, Chicago and London, 438 pp.
- Selitskaya, V. I. (1962), The 24-hour and annual variation of meteorological elements in the lower layer of air at 015 km above the Voeikova settlement, *Trudy GGO.*, No. 135.
- Staley, D. O. and G. M. Jurica (1968), Radiative modification of selected vertical temperature distributions, *Quart. J. Roy. Meteorol. Soc.*, 94, 310-317.
- Sutton, O. G. (1953), *Micrometeorology*, McGraw-Hill Book Co., Inc., New York 33 pp.
- U. S. Dept. of Commerce (1966-7), *Local Climatological Data, Annual Summary for Oklahoma City, Oklahoma*, U. S. Government Printing Office, Washington, D.C.

U. S. Dept. of Commerce (1966-7), Daily Weather Maps, December 9, 1966 to May 31, 1967, U. S. Government Printing Office, Washington, D. C.

Warner, J. and J. W. Telford (1964), Fluxes of heat and vapor in the lower atmosphere derived from aircraft observations, J. Atmos. Sci., 21, 539-548.

_____, (1967), Convection below cloud base, J. Atmos. Sci., 24, 374-382.

Weber, A. H. and L. D. Sanders (1970), Evaluation of roughness lengths at the NSSL-WKY meteorological tower, ESSA Tech. Memo. ERLTM-NSSL 47, 24 pp.

APPENDIX

Temperatures are measured through a composite of two independent systems - an ambient and a delta system. Ambient temperatures are measured at the surface level and level 6 and are recorded on one strip chart recorder with a range of $\pm 25^{\circ}\text{C}$ (fig. A-1). Temperatures in the delta system are referenced to a thermistor at level 6 (444 m). They are measured at the surface level and at levels 1-5 and are recorded on a second strip chart recorder with a range of $\pm 10^{\circ}\text{C}$ (fig. A-2).

To obtain the true temperature at each level, a calibration correction must be applied to each thermistor. The correction curves are a sinusoidal function of temperature (fig. A-3) and vary from thermistor to thermistor. These corrections are determined in a laboratory experiment before and after a data collection period, as mentioned in the main body of the text. The experiment consists of immersing the probes in an agitated water bath that is insulated from the ambient air. A high quality, calibrated, liquid-in-glass thermometer is also immersed in the water, and thermistor readings are compared to the liquid-in-glass thermometer. The corrections A_i and D_i given below are the negative of the deviation of the thermistor from the calibration thermometer. The temperature of the water bath is varied slowly and readings are made about every 5°C .

The true temperature (T_6) at level 6 is simply

$$T_6 = T_6' + A_6 , \quad (\text{A-1})$$

where T_6' is measured temperature and A_6 the calibration correction at T_6' for that ambient system thermistor.

Since temperature is not recorded at level 6 in the delta system, the correction for the level 6 delta thermistor, D_6 , is subtracted from T_6 to obtain an uncorrected temperature for the level 6 reference thermistor:

$$T_6'' = T_6 - D_6 . \quad (\text{A-2})$$

Temperatures at the surface and at levels 1-5 are then obtained using the relationship:

$$T_i = (T_i' + T_6'') + D_i , \quad (\text{A-3})$$

where T_i' is the temperature difference from the reference thermistor measured at level i.

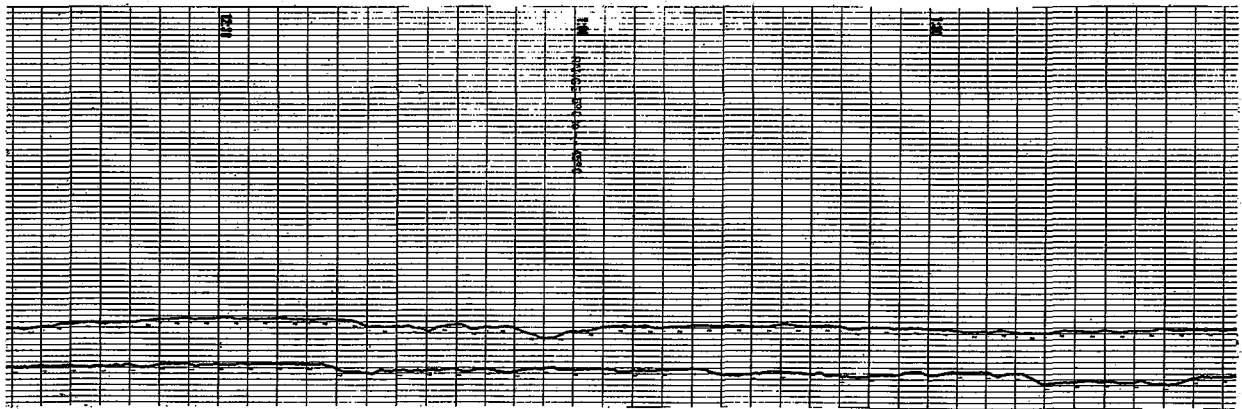


Figure A-1. Temperature strip chart in the ambient mode.

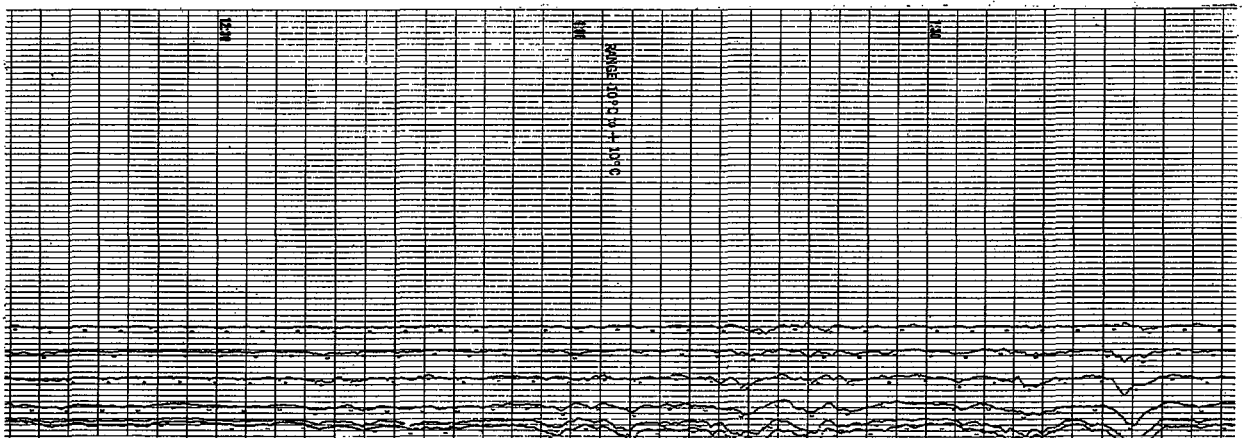


Figure A-2. Temperature strip chart in the delta mode.

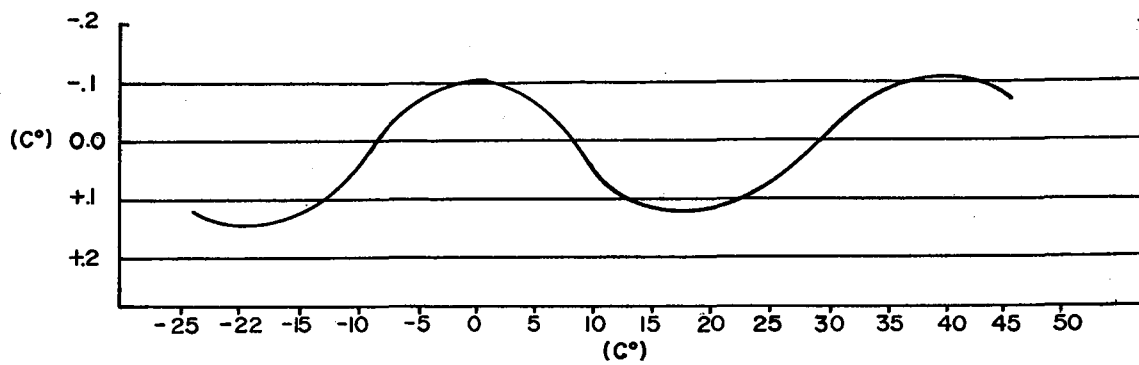


Figure A-3. Nominal linearity correction for a typical thermistor (range -25°C to 50°C).

A true temperature is also obtained at the surface level from the ambient system in a manner analogous to A-1. The two surface temperatures provide a check on the two independent systems.

The data were reduced from the strip charts to digital form with the aid of a Benson-Lehner Oscar Model K trace reader. With this equipment, there was uncertainty in the base line alignment amounting to a $\pm .25^{\circ}\text{C}$ on ambient charts and $\pm .10^{\circ}\text{C}$ on delta charts. The resolution uncertainty for smooth traces (e.g., fig. A-2) was about $\pm .12^{\circ}\text{C}$ and $\pm .05^{\circ}\text{C}$ on the ambient and delta charts, respectively. Finally, considering average calibration corrections for the thermistors of about $\pm .02^{\circ}\text{C}$, the total uncertainty in the ambient mode was $\pm .39^{\circ}\text{C}$ and in the delta mode $\pm .17^{\circ}\text{C}$. This meant that there was a possible error of $\pm .56^{\circ}\text{C}$ in derived temperatures obtained through the delta system. In unsmooth traces, the uncertainty is slightly higher.

Because of these rather large uncertainties, the data were subjected to an intensive quality control procedure. Three basic checks were made:

- (1) The difference between the two surface temperatures,
- (2) Large values of the ambient lapse rate,
- (3) Large values of $\Delta T \text{ hr}^{-1}$.

The two surface temperature measurements should be very close when proper calibration corrections are added. If not, one or more of three thermistor values may have been erroneously digitized (surface ambient, surface delta, or level 6 ambient), although the discrepancies may have been of a mechanical origin.

The second quality control technique makes use of some general meteorological behavior. On days when there is strong surface heating, heat conduction causes the temperature profile near the surface to be typically logarithmic. Further aloft the profile tends to vary about the dry adiabatic lapse rate (below the lifting condensation level). Lapse rates steeper than dry adiabatic occur, but they are short lived in most cases and are averaged out in a mean computed from a long record. Under these quasi-steady conditions, the upper layers can be checked for excessively large positive lapse rates. The technique is most useful during the day but can also be employed at night, especially on cloudy nights when the vertical temperature gradient is positive. With inversions, the technique is not effective.

Technique (3) is not as useful as the previous two because large values of $\Delta T \text{ hr}^{-1}$ (the temperature difference between two observations) are often real during sunrise and sunset periods, frontal passages, at the onset of precipitation and in the presence of gravity waves in strong inversions. Any large values that occurred and could not be explained by the above causes were closely investigated.

When the temperature data were quality controlled, a sizeable number of discrepancies were noted. A small sample was redigitized and additional discrepancies from the original data set were found. It was then decided that the whole sample should be rechecked. The strip charts were carefully inspected and compared to the machine digitized values by the authors, further revealing many discrepancies, most of which seemed to be base line errors. In rechecking the data by inspection, the base line error and error inherent in the reader were eliminated. Because the traces were frequently smooth, a 5 min mean often could be visually determined to within the resolution error.

The combined uncertainties caused by resolution and estimating the mean were thought to be seldom larger than $\pm .20^{\circ}\text{C}$ in the ambient system and $\pm .15^{\circ}\text{C}$ in the delta system. Combining this with the calibration correction error of $\pm .02^{\circ}\text{C}$, the resulting temperature was generally within $\pm .39^{\circ}\text{C}$ of the true temperature.

After redigitizing by hand, the quality control checks were rerun and some further rechecking of the data was done. In the final form the mean difference between the two surface temperatures (quality control check number 1) for the entire set was $.03^{\circ}\text{C}$. Finally, level 3 appeared to be biased by $.07$ to $.10^{\circ}\text{C}$. A faulty aspirator could be a likely source of this bias. Extensive checking showed, however, that this bias was not favored by any particular time or for any particular air mass, cloud cover, wind speed or wind direction.

NATIONAL SEVERE STORMS LABORATORY

The NSSL Technical Memoranda, beginning with No. 28, continue the sequence established by the U. S. Weather Bureau National Severe Storms Project, Kansas City, Missouri. Numbers 1-22 were designated NSSL Reports. Numbers 23-27 were NSSL Reports, and 24-27 appeared as subseries of Weather Bureau Technical Notes. These reports are available from the National Technical Information Service, Operations Division, Springfield, Virginia 22151, for \$3.00, and a microfiche version for \$0.95. NTIS numbers are given below in parentheses.

- No. 1 National Severe Storms Project Objectives and Basic Design. Staff, NSSL. March 1961. (PB-168207)
- No. 2 The Development of Aircraft Investigations of Squall Lines from 1956-1960. B. B. Goddard. (PB-168208)
- No. 3 Instability Lines and Their Environments as Shown by Aircraft Soundings and Quasi-Horizontal Traverses. D. T. Williams. February 1962. (PB-168209)
- No. 4 On the Mechanics of the Tornado. J. R. Fulks. February 1962. (PB-168210)
- No. 5 A Summary of Field Operations and Data Collection by the National Severe Storms Project in Spring 1961. J. T. Lee. March 1962. (PB-165095)
- No. 6 Index to the NSSL Surface Network. T. Fujita. April 1962. (PB-168212)
- No. 7 The Vertical Structure of Three Dry Lines as Revealed by Aircraft Traverses. E. L. McGuire. April 1962. (PB-168213)
- No. 8 Radar Observations of a Tornado Thunderstorm in Vertical Section. Ralph J. Donaldson, Jr. April 1962. (PB-174859)
- No. 9 Dynamics of Severe Convective Storms. Chester W. Newton. July 1962. (PB-163319)
- No. 10 Some Measured Characteristics of Severe Storms Turbulence. Roy Steiner and Richard H. Rhyne. July 1962. (N62-16401)
- No. 11 A Study of the Kinematic Properties of Certain Small-Scale Systems. D. T. Williams. October 1962. (PB-168216)
- No. 12 Analysis of the Severe Weather Factor in Automatic Control of Air Route Traffic. W. Boynton Beckwith. December 1962. (PB-168217)
- No. 13 500-Kc./Sec. Sferics Studies in Severe Storms. Douglas A. Kohl and John E. Miller. April 1963. (PB-168218)
- No. 14 Field Operations of the National Severe Storms Project in Spring 1962. L. D. Sanders. May 1963. (PB-168219)
- No. 15 Penetrations of Thunderstorms by an Aircraft Flying at Supersonic Speeds. G. P. Roys. Radar Photographs and Gust Loads in Three Storms of 1961 Rough Rider. Paul W. J. Schumacher. May 1963. (PB-168220)
- No. 16 Analysis of Selected Aircraft Data from NSSL Operations, 1962. T. Fujita. May 1963. (PB-168221)
- No. 17 Analysis of Methods for Small-Scale Surface Network Data. D. T. Williams. August 1963. (PB-168222)
- No. 18 The Thunderstorm Wake of May 4, 1961. D. T. Williams. August 1963. (PB-168223)
- No. 19 Measurements by Aircraft of Condensed Water in Great Plains Thunderstorms. George P. Roys and Edwin Kessler. July 1966. (PB-173048)
- No. 20 Field Operations of the National Severe Storms Project in Spring 1963. J. T. Lee, L. D. Sanders and D. T. Williams. January 1964. (PB-168224)
- No. 21 On the Motion and Predictability of Convective Systems as Related to the Upper Winds in a Case of Small Turning of Wind with Height. James C. Fankhauser. January 1964. (PB-168225)
- No. 22 Movement and Development Patterns of Convective Storms and Forecasting the Probability of Storm Passage at a Given Location. Chester W. Newton and James C. Fankhauser. January 1964. (PB-168226)
- No. 23 Purposes and Programs of the National Severe Storms Laboratory, Norman, Oklahoma. Edwin Kessler. December 1964. (PB-166675)
- No. 24 Papers on Weather Radar, Atmospheric Turbulence, Sferics, and Data Processing. August 1965. (AD-621586)
- No. 25 A Comparison of Kinematically Computed Precipitation with Observed Convective Rainfall. James C. Fankhauser. September 1965. (PB-168445).

- No. 26 Probing Air Motion by Doppler Analysis of Radar Clear Air Returns. Roger M. Lhermitte. May 1966. (PB-170636)
- No. 27 Statistical Properties of Radar Echo Patterns and the Radar Echo Process. Larry Armijo. May 1966. The Role of the Kutta-Joukowski Force in Cloud Systems with Circulation. J. L. Goldman. May 1966. (PB-170756)
- No. 28 Movement and Predictability of Radar Echoes. James Warren Wilson. November 1966. (PB-173972)
- No. 29 Notes on Thunderstorm Motions, Heights, and Circulations. T. W. Harrold, W. T. Roach, and Kenneth E. Wilk. November 1966. (AD-644899)
- No. 30 Turbulence in Clear Air Near Thunderstorms. Anne Burns, Terence W. Harrold, Jack Burnham, and Clifford S. Spavins. December 1966. (PB-173992)
- No. 31 Study of a Left-Moving Thunderstorm of 23 April 1964. George R. Hammond. April 1967. (PB-174681)
- No. 32 Thunderstorm Circulations and Turbulence from Aircraft and Radar Data. James C. Fankhauser and J. T. Lee. April 1967. (PB-174860)
- No. 33 On the Continuity of Water Substance. Edwin Kessler. April 1967. (PB-175840)
- No. 34 Note on the Probing Balloon Motion by Doppler Radar. Roger M. Lhermitte. July 1967. (PB-175930)
- No. 35 A Theory for the Determination of Wind and Precipitation Velocities with Doppler Radars. Larry Armijo. August 1967. (PB-176376)
- No. 36 A Preliminary Evaluation of the F-100 Rough Rider Turbulence Measurement System. U. O. Lappe. October 1967. (PB-177037)
- No. 37 Preliminary Quantitative Analysis of Airborne Weather Radar. Lester P. Merritt. December 1967. (PB-177188)
- No. 38 On the Source of Thunderstorm Rotation. Stanley L. Barnes. March 1968. (PB-178990)
- No. 39 Thunderstorm - Environment Interactions Revealed by Chaff Trajectories in the Mid-Troposphere. James C. Fankhauser. June 1968. (PB-179659)
- No. 40 Objective Detection and Correction of Errors in Radiosonde Data. Rex L. Inman. June 1968. (PB-180284)
- No. 41 Structure and Movement of the Severe Thunderstorms of 3 April 1964 as Revealed from Radar and Surface Mesonet Data Analysis. Jess Charba and Yoshikazu Sasaki. October 1968. (PB-183310)
- No. 42 A Rainfall Rate Sensor. Brian E. Morgan. November 1968. (PB-183979)
- No. 43 Detection and Presentation of Severe Thunderstorms by Airborne and Ground-Based Radars: A Comparative Study. Kenneth E. Wilk, John K. Carter, and J. T. Dooley. February 1969. (PB-183572)
- No. 44 A Study of a Severe Local Storm of 16 April 1967. George Thomas Haglund. May 1969. (PB-184-970)
- No. 45 On the Relationship Between Horizontal Moisture Convergence and Convective Cloud Formation. Horace R. Hudson. March 1970. (PB-191720)
- No. 46 Severe Thunderstorm Radar Echo Motion and Related Weather Events Hazardous to Aviation Operations. Peter A. Barclay and Kenneth E. Wilk. June 1970. (PB-192498)
- No. 47 Evaluation of Roughness Lengths at the NSSL-WKY Meteorological Tower. Leslie D. Sanders and Allen H. Weber. August 1970. (PB-194587)
- No. 48 Behavior of Winds in the Lowest 1500 ft in Central Oklahoma: June 1966 - May 1967. Kenneth C. Crawford and Horace R. Hudson. August 1970.
- No. 49 Tornado Incidence Maps. Arnold Court. August 1970. (COM-71-00019)
- No. 50 The Meteorologically Instrumented WKY-TV Tower Facility. John K. Carter. September 1970. (COM-71-00108)
- No. 51 Papers on Operational Objective Analysis Schemes at the National Severe Storms Forecast Center. Rex L. Inman. November 1970. (COM-71-00136)
- No. 52 The Exploration of Certain Features of Tornado Dynamics Using a Laboratory Model. Neil B. Ward. November 1970. (COM-71-00139)
- No. 53 Rawinsonde Observation and Processing Techniques at the National Severe Storms Laboratory. Stanley L. Barnes, James H. Henderson and Robert J. Ketchum. April 1971.

No. 54 Model of Precipitation and Vertical Air Currents. Edwin Kessler and William C. Bumgarner. June 1971.

No. 55 The NSSL Surface Network and Observations of Hazardous Wind Gusts. Operations Staff. June 1971.

No. 56 Pilot Chaff Project at the National Severe Storms Laboratory. Edward A. Jessup. November 1971.

No. 57 Numerical Simulation of Convective Vortices. Robert P. Davies-Jones and Glenn T. Vickers. November 1971.